This is to certify that the

dissertation entitled

DEVELOPMENT OF AN ACTIVE ACOUSTIC SINK (AAS)

FOR NOISE CONTROL IN ACOUSTIC SPACES

presented by

SACHIN D. GOGATE

has been accepted towards fulfillment
of the requirements for

Ph.D. degree in Mechanical Engineering

Clark Radcliffe
Major professor

Date Sept 1, 1995

DEVELOPMENT OF AN ACTIVE ACOUSTIC SINK (AAS) FOR NOISE CONTROL IN ACOUSTIC SPACES

By

Sachin D. Gogate

A DISSERTATION

Submitted to
Michigan State University
in partial fulfillment of the requirements
for the degree of

DOCTOR OF PHILOSOPHY

Department of Mechanical Engineering

1995

acou

canc

prin

origi

Sour

encl

abso

acou

acou

spea

meth

on a

then

press

Expe

ABSTRACT

DEVELOPMENT OF AN ACTIVE ACOUSTIC SINK (AAS) FOR NOISE CONTROL IN ACOUSTIC SPACES

By

Sachin D. Gogate

Active control of undesirable acoustic noise satisifies one of the two distinct acoustic design objectives : sound cancellation and sound power absorption. Sound cancellation has been traditionally used for control of acoustic noise. It works on the principle of destructive interference of sound fields and is achieved by superimposing an original sound field with an electroacoustically generated sound field of opposite phase. Sound power absorption is achieved by removing acoustic energy due to noise from an enclosed space.

Active Acoustic Sink (AAS), an active noise control system based on sound power absorption is developed in this work. It uses speaker to absorb acoustic energy from an acoustic volume. The speaker velocity must track speaker face acoustic pressure to ensure acoustic energy flow in the speaker.

The three stages of research discussed in this work are speaker dynamic modeling, speaker compensation design, and AAS controller design. In the first stage, a methodology for constructing a speaker model is developed and experimentally verified on a dual-wound coil subwoofer. Velocity feedback compensation for the subwoofer is then designed in the next stage to ensure speaker cone velocity tracking of speaker face pressure. The AAS controller is designed, implemented, and tested in the final stage. Experimental tests of AAS indicate successful performance.

To Sou. Aai

and advice, I

Dedication

To Sou. Aai, Ti. Dada, Sou. Shubhatai and Suchatai without whose help, encouragement, and advice, I would not have come this far.

Copyright

I wou

not only his

also like to t

have been im

I wou

FitzSimons,

during my stu

I woul

during my stu

I grate

the fixtures ne

I would

Sanjay Mishra

the darkest tim

been technical

friends, Dr. Sa

Prasad, Nandu,

I would

over the years.

Ruth Andersland

Acknowledgments

I would like to express my sincere appreciation to Professor Clark J. Radcliffe for not only his technical advice but also for his valuable tips on professional skills. I would also like to thank him for the generous financial support without which this study would have been impossible.

I would like to thank my committee members, Professors C. MacCluer, P.M. FitzSimons, A. G. Haddow and R. C. Rosenberg for their advice, comments and help during my studies here.

I would like to thank my parents and sisters for their encouragement and support during my studies at Michigan State University.

I gratefully acknowledge the assistance of Bob Rose and Leonard Eisele who made the fixtures necessary for the experiments in this work.

I would like to give special thanks to my roommates at MSU, Manoj Thatte and Sanjay Mishra. I cannot express in words their valuable contribution and support during the darkest times of dissertation. Although the support they have given me has not always been technical, I feel that it has made me a better person. Thanks also go to my dear friends, Dr. Sanjeev Kholkute, Shanti Vedula, Uma Iyer, Hari, Yogesh Pathak, Shail, Prasad, Nandu, Venky and Pratima. You all have made my life at MSU an enjoyable one.

I would like to thank my officemate, XianLi Huang for his friendship and help over the years. I would also like to thank my friends, Jerome Palazzolo, Byam Brooks, Ruth Andersland, and Chang-po Chao for making my stay at MSU enjoyable.

TABLE OF CONTENTS

LIST OF TABLES

LIST OF FIGURES

1.1. Overvie

Noise

High noise l

environment.

years as peop

often necessa

1.2. Previous

Contr

methods. Pa

Shuku, et al.

wavelength is

effective frequ

done based or

(Crocker et al

material is qui

Small structur

structural damp

Chapter 1 Introduction

1.1. Overview

Noise control can produce quiet environments that are comfortable and productive. High noise levels in work areas are perceived as indicators of an inferior working environment. The reduction of undesirable noise has been gaining attention over recent years as people are becoming more and more noise conscious. The reduction of noise is often necessary in power plants, factories and passenger compartment of vehicles.

1.2. Previous work

Control of acoustic noise is conventionally achieved by either passive or active methods. Passive noise control using sound absorptive material (Crocker, et al., 1982, Shuku, et al. 1972, Ling, 1993) does not work well at low frequencies where the sound wavelength is large compared to the treatment thickness. Figure 1.1 shows the minimum effective frequency for absorptive materials at different thicknesses. The computation is done based on half-power point frequencies of material acoustic absorption coefficients (Crocker et al., 1982). The sound control effectiveness of a 2 inch thick absorption material is quite limited below 400 Hz and decreases rapidly with decreasing frequency. Small structural velocities at low frequencies also limit the effectiveness of passive structural damping treatments (Joachim et al., 1981).

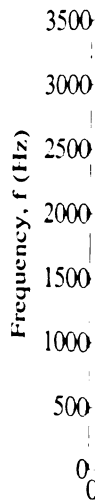

Figure 1.1. N
Different Th

Active
original prima
opposite phase
Paul Leug wa
published in U
has been prese
picked up by c
one or more lo
primary unwan
noise cancellat
They described

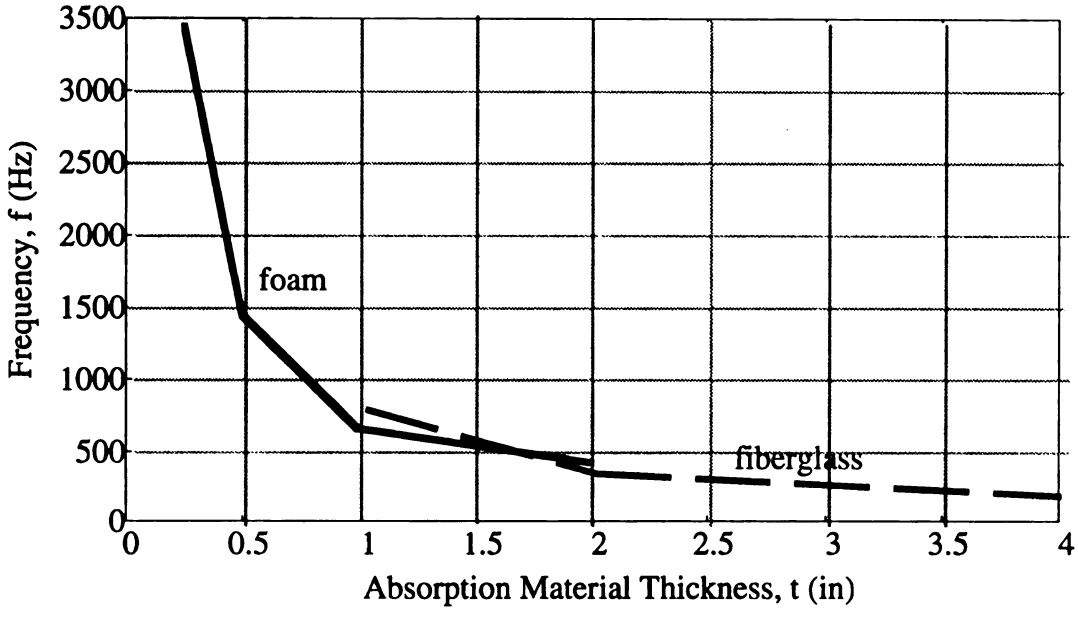

Figure 1.1. Minimum Effective Frequency for Polyurethane Foam and Fibrous Glass at Different Thickness (From "Noise and Vibration Control" by M.J. Crocker, and F.M. Kessler, Vol. II, 1982, pg. 23.

Active noise control using noise cancellation is achieved by superimposing the original primary sound field with an electroacoustically generated secondary field of opposite phase. It works on the principle of destructive sound fields. German inventor Paul Leug was the first person to describe the idea of sound cancellation in his patent published in United States in 1936 (Figure 1.2). A historical discussion of Leug's work has been presented by Guicking (1990). According to his principle, the unwanted sound is picked up by one or more microphones, their electrical signal fed, after amplification, to one or more loudspeakers so that the sound wave produced is in opposing phase to the primary unwanted sound and cancels it. Olson and May (1953) described a similar active noise cancellation system which they misleadingly called an electronic sound absorber. They described a system for actively canceling the sound detected by a microphone, which

is placed clos

time as Olso

acoustic noise

at even harmo

a harmonic so

the amplitude

particular dire

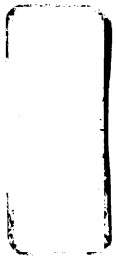

Figure 1.2. Di

"On the inv

Aco

is placed close to a loudspeaker acting as a secondary source (Figure 1.3). About the same time as Olson and May, William Conover (1956) demonstrated active reduction of acoustic noise from large main transformers. The sound radiated by these transformers is at even harmonics of the line frequency. Conover in his control system (Figure 1.4) used a harmonic source generated from the transformer's line voltage. He manually adjusted the amplitude and phase of the harmonic source signal to cancel the acoustic pressure in a particular direction away from the transformer.

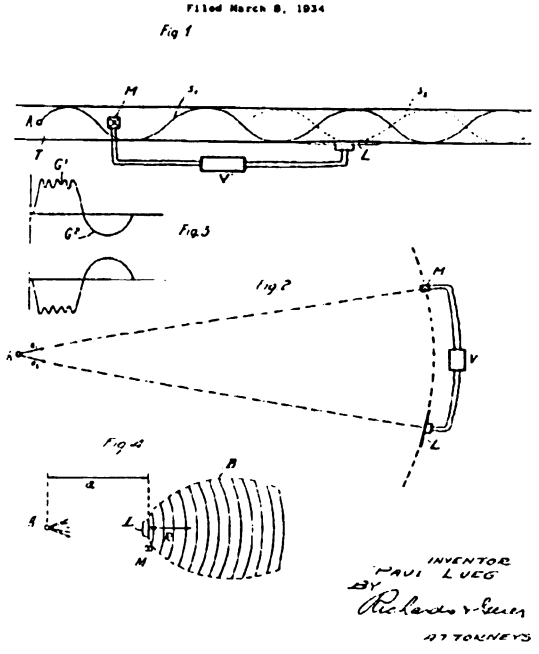

Figure 1.2. Diagrams Describing Paul Leug's Patent on Active Noise Cancellation (From "On the invention of active noise control by Paul Leug", by D. Guicking, Journal of Acoustical Society of America, Vol. 87, No. 5, 1990, pp. 2251-2253)

Figure 1.3. T

"Electronic S

Figure 1.4. Ma

(From "Fighting

The adver

to realize these no

systems based on

interior noise contr

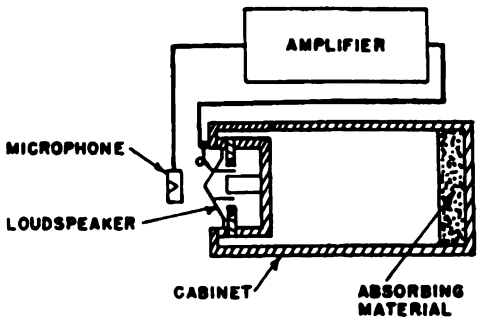

Figure 1.3. The Active Sound Cancellation Device constructed by Olson and May (From "Electronic Sound Absorber", by H.F. Olson and E.G. May, Journal of Acoustical Society of America, Vol. 25., No.6, 1953, pp. 1130-1136)

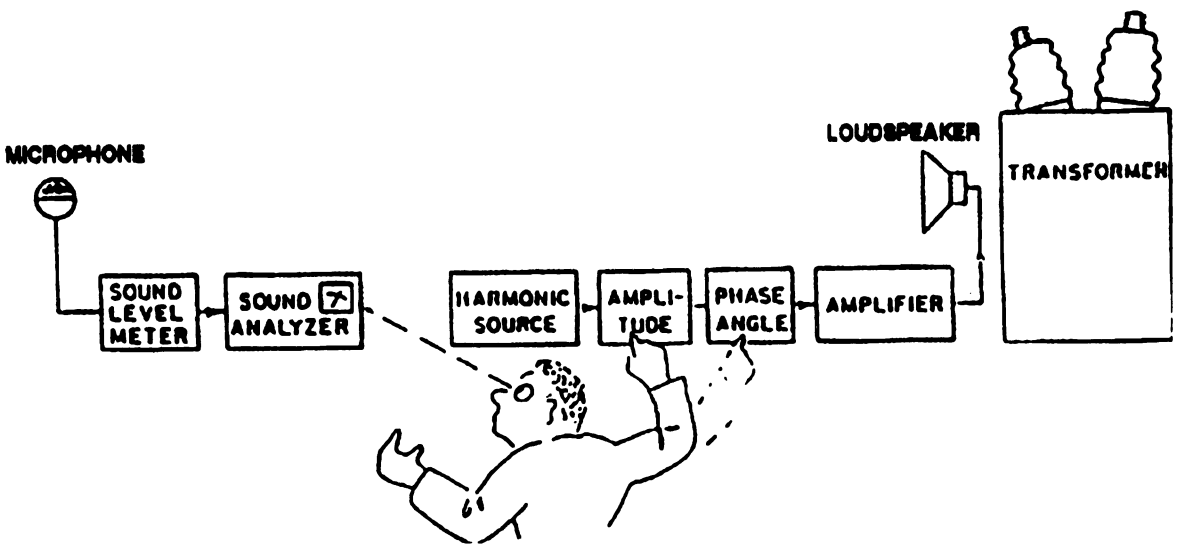

Figure 1.4. Manually Adaptive Active Noise Cancellation System proposed by Conover (From "Fighting Noise with Noise", by W.B. Conover, Noise Control 2, 1956, pp. 78-82)

The advent of digital signal processing techniques and devices has made it possible to realize these noise cancellation algorithms in practice. A number of active noise control systems based on the principle of sound cancellation have been developed for vehicle interior noise control (Costin et al., 1989, Elliot et al., 1990, Sutton et al., 1990, Bao et al.,

1991) and duct noise control (Manjal and Eriksson, 1988, Eriksson et al., 1988, Swinbanks, 1973) These control systems use sensor microphones for measurement of acoustic noise and generate "antinoise" through audio speakers driven by an adaptive algorithm. The "antinoise" cancels the correlated acoustic noise at measurement microphone locations. The acoustical effect of noise cancellation at microphones is to generate "zones of silence" around these locations. It has been observed that the spatial extent of "zones of silence" is of the order of one-tenth of an acoustic wavelength (3.4 m at 100 Hz) and rapidly decreases as the frequency of noise increases above 200 Hz (Elliot et al., 1988). Beyond these "zones of silence", sound cancellation may even increase the resulting noise at some locations.

1.3. A Novel Noise Control Technique

Active Acoustic Sink (AAS), an active noise control system, based on the objective of sound power absorption is proposed in this work (Radcliffe et al. 1994, Hall, 1994)). Sound power is the rate at which energy is radiated and is described by sound intensity which measures energy flow per unit area. The AAS (Figure 1.1) will use an electromechanical speaker as a control actuator to absorb acoustic energy. The instantaneous acoustic intensity, $\mathbf{I_i}$, at the speaker face is the product of acoustic pressure, p, and particle velocity, v.

$$\mathbf{I_i} = pv = \frac{1}{A_{spkr}} p_{face} q_{spkr} \tag{1.1}$$

Here the acoustic pressure is equated to speaker face pressure, p_{face}, and acoustic particle velocity is related to speaker volumetric flow rate, q_{spkr}, and the effective area of the speaker, A_{spkr}. A microphone placed at the speaker face measures the total acoustic pressure, p_{face}. The AAS theory for absorption of acoustic energy by the speaker (Radcliffe and Gogate, 1995) generates negative instantaneous acoustic intensity by requiring that speaker volumetric flow rate track the negative of speaker face pressure.

$$q_{spkr} = -Kp_{face} \tag{1.2}$$

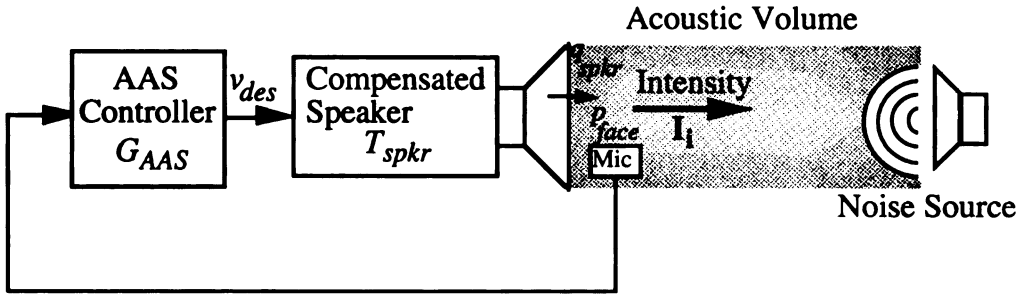

Figure 1.5. Schematic of the Active Acoustic Sink System

The AAS controller, G_{AAS}, is designed to realize the AAS objective (1.2). The instantaneous acoustic intensity at the speaker face can then be expressed as

$$\mathbf{I_i} = -\frac{K}{A_{spkr}} p_{face}^2 \tag{1.3}$$

For $K > 0$, acoustic power flux will always be directed into, and absorbed by, the speaker face. As the magnitude of K is increased, more power flux will be directed into the speaker face. The speaker behaves as active acoustic sink because any external noise source located near the speaker will have its local acoustic intensity directed into the speaker. The AAS can be ideally thought of as an acoustic black hole where acoustic energy due to external noise at the face of AAS will not be reflected. The AAS system generates negative, non-zero intensity, $\mathbf{I_i}$, from non-zero acoustic pressure, p_{face}. Active cancellation systems use "anti-noise" to generate zero-valued face pressure resulting in zero acoustic intensity. This result indicates a fundamental difference between the dissipative AAS approach and the non-dissipative "anti-noise" approach to active noise control.

The AAS objective (1.2) requires speaker volumetric flow rate to track the speaker face pressure with minimal magnitude and phase error over the controller bandwidth. This is critical if AAS is to be successfully used for wide band noise control applications. A

typical electromechanical speaker has a non-constant voltage-to-velocity frequency response due to the speaker free-air resonance. This varying velocity response does not allow the uncompensated speaker volumetric flow rate to accurately track a desired input signal. Speaker compensation is therefore necessary to overcome this problem and allows a compensated speaker to be used as a control actuator in AAS (Radcliffe and Gogate, 1996).

The successful performance of speaker velocity compensation depends on accurate measurement of speaker cone velocity. The velocity measurement is done in this work using a novel voice coil sensor and no external components. The design of the voice coil sensor is based on an accurate speaker model which precisely predicts the measured speaker dynamics (Radcliffe and Gogate 1995). It is the iterative process of model development that is key to the successful AAS and velocity compensation development. The identification of speaker dynamics is therefore essential in AAS.

The design stages of AAS include modeling and identifying speaker dynamics, developing the speaker compensation design, and developing the control model and AAS system. The final stage involves construction, implementation and testing of the active acoustic sink controller.

1.4. Chapter Summary

Chapter 2 develops a dynamic model of an electromechanical speakers to be used as control actuator in AAS. The data from speaker manufacturers do not always provide the parameters required to construct a speaker dynamic model. A simple laboratory based methodology for identifying the speaker parameters is also presented in this chapter. The method is experimentally verified on an enclosed dual-wound coil subwoofer speaker.

Chapter 3 develops a velocity feedback compensation designed to minimize magnitude and phase variations in speaker velocity response. Electromechanical speakers have a non-constant velocity frequency response. This makes them poor control actuators unless appropriate compensation is provided for their varying velocity response. Velocity

feedback compensation for a dual-wound coil subwoofer speaker is presented in this chapter. It uses a proportional compensator and a novel speaker cone velocity sensor.

Chapter 4 develops an analytical model of AAS controller using a compensated speaker model and an acoustic model of enclosed space. The AAS controller is designed to give an acoustically absorptive surface at the cone of compensated speaker by generating a negative, real acoustic impedance at the speaker face. A stability analysis is performed to verify that the controller model results in a stable closed loop AAS system.

Chapter 5 discusses the implementation and testing of the AAS system. Experimental tests of the AAS indicate successful performance.

Chapter 6 summarizes the dissertation and discusses directions for future research.

Chapter 2 Identification and Modeling of Speaker Dynamics

2.1. Introduction

Electromechanical speakers are commonly used as control actuators in many acoustic control applications (Hull et al., 1990). Control of acoustic system behavior over a specified bandwidth requires precise knowledge of speaker dynamics. This is essential because often the speaker actuator bandwidth falls within the bandwidth of the acoustic system for a realistic controller. The data from speaker manufacturers do not always provide the parameters required to construct a speaker dynamic model. IEEE std. 219-1975 gives methods to estimate the speaker parameters (Beranek, 1986, and Colloms, 1985) when partial information is provided by manufacturer, however, the standard procedures are tedious. A simple laboratory based methodology for identifying the speaker parameters of a dual-wound coil subwoofer speaker is presented in this chapter. The methodology is validated by comparing the model and measured voltage-to-velocity subwoofer responses. The effect of speaker enclosures is also discussed.

2.2. Modeling a Dual-Wound Coil Subwoofer Speaker

Dual-wound coil subwoofer (Figure 2.1) is common in the audio industry. It is an electromechanical speaker (Figure 2.2) consisting of electrical, mechanical and acoustic components. The dual-wound coil design consists of primary and secondary coils wound on a bobbin connected to the speaker cone. The 12 inch (30 cm) subwoofer used in this work (Radio Shack Realistic model 40-1350) is driven through the primary coil of the speaker. As the drive voltage is applied to the primary coil, the varying electromagnetic field produced around the primary coil interacts with the magnetic field produced by a

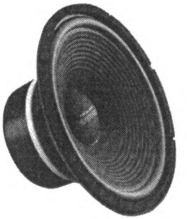

Figure 2.1. Radio Shack Realistic 12 inch, Dual-Wound, Subwoofer Model 40-1350

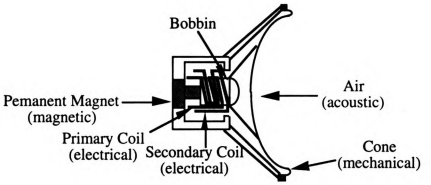

Figure 2.2. Schematic Representation of a Dual-Wound Coil Subwoofer Speaker

fixed permanent magnet. The interaction between the two magnetic fields produces a mechanical force in the primary coil attached to the speaker cone. The voltage in the speaker cone's secondary coil is induced by both the velocity of the coil in the speaker magnet's electromagnetic field and the mutual inductance between primary and secondary coils.

An analytical model of the dual-wound coil subwoofer speaker can be developed (Figure 2.3) by using the power summation and energy conservation principles of the

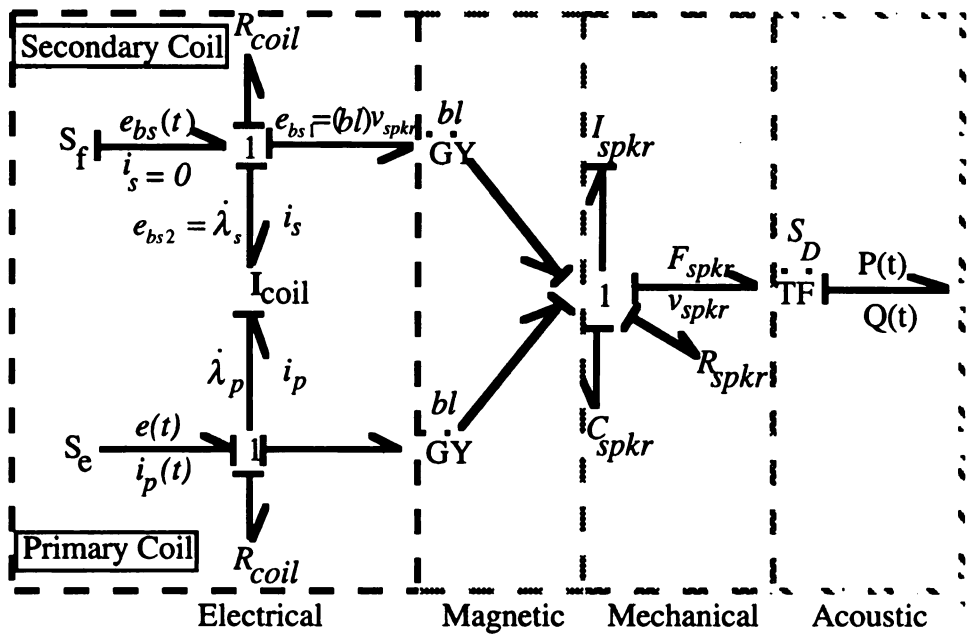

Figure 2.3. Bond Graph Model of a Dual-Wound Coil Subwoofer Speaker without Enclosure

Bond Graph methodology (Rosenberg and Karnopp, 1983). The Bond Graph arrows represent power flow from the electrical voltage, S_e, applied at primary coil through the model's elements. Dual-wound coils are represented here as a multiport $\mathbf{I}_{coil}$ field in the bond graph model. The electrical power is either dissipated, transformed or stored in the model elements. Power is dissipated in resistive elements $R_{coil}$and R_{spkr}, and transformed both from electrical to mechanical power in the 'GY' element and from mechanical to acoustic power in the 'TF' element. Power is stored as kinetic energy in the 'I' elements and as potential energy in the 'C' elements. The open circuit on secondary coil is represented by secondary coil current, $i_s = 0$ imposed by the source of flow, S_f.

The energy variables in the bond graph model include coil flux linkages, λ_p and λ_s, speaker cone displacement, x_{spkr} and speaker cone velocity, v_{spkr}. A linear

approximation is used to relate the flux linkages, λ_p and λ_s, of multiport $\mathbf{I}_{\text{coil}}$ field to the port currents i_p and i_s in primary and secondary coils.

$$\lambda = \mathbf{I}i \tag{2.1}$$

where, $\mathbf{I} = \begin{bmatrix} I_{coil,p} & M_{coil,p} \\ M_{coil,s} & I_{coil,s} \end{bmatrix}$ is the inductance matrix, $i = \begin{pmatrix} i_p \\ i_s \end{pmatrix}$ is the vector of port currents and $\lambda = \begin{pmatrix} \lambda_p \\ \lambda_s \end{pmatrix}$ is the vector of coil flux linkages. $I_{coil,p}$ and $I_{coil,s}$ in the inductance matrix are the self inductances of primary and secondary coils, whereas, $M_{coil,p}$ and $M_{coil,s}$ are the mutual inductances between primary and secondary coils. The self and mutual inductance terms in the inductance matrix are equal for audio dual-wound speakers because the coils are designed to be identical in construction.

$$M_{coil,p} = M_{coil,s} = M_{coil} \tag{2.2}$$

$$I_{coil,p} = I_{coil,s} = I_{coil} \tag{2.3}$$

The speaker equations can be written from the bond graph in state space form by choosing energy variables as state variables and appropriate input and output variables. The input variables are speaker drive voltage, $e(t)$, and acoustic pressure, $P(t)$. The output variables are speaker volumetric flow rate, $Q(t)$ and speaker drive current in the primary coil, $i_p(t)$.

$$\frac{\mathrm{d}}{\mathrm{dt}}\begin{pmatrix} x_{spkr} \\ v_{spkr} \\ \lambda_p \end{pmatrix} = \begin{bmatrix} 0 & 1 & 0 \\ \dfrac{-1}{C_{spkr}I_{spkr}} & \dfrac{-R_{spkr}}{I_{spkr}} & \dfrac{bl}{\left(I_{spkr}I_{coil}\right)} \\ 0 & -bl & \dfrac{-R_{coil}}{I_{coil}} \end{bmatrix}\begin{pmatrix} x_{spkr} \\ v_{spkr} \\ \lambda_p \end{pmatrix} + \begin{bmatrix} 0 & 0 \\ 0 & \dfrac{-S_D}{I_{spkr}} \\ 1 & 0 \end{bmatrix}\begin{pmatrix} e(t) \\ P(t) \end{pmatrix} \tag{2.4a}$$

$$\begin{pmatrix} Q(t) \\ i_p(t) \end{pmatrix} = \begin{bmatrix} 0 & S_D & 0 \\ 0 & 0 & \frac{1}{I_{coil}} \end{bmatrix} \begin{pmatrix} x_{spkr} \\ v_{spkr} \\ \lambda_p \end{pmatrix} \tag{2.4b}$$

The voltage, $e_{bs}(t)$, introduced in the secondary speaker coil is obtained from the bond graph model (Figure 2.3) by summing the voltages across 1-junction on secondary coil side. These voltages include the voltage, $e_{bs1}(t)$, due to the mechanical motion of speaker cone and the voltage, $e_{bs2}(t)$ due to the mutual inductance, M_{coil}, between the coils.

$$e_{bs}(t) = e_{bs1}(t) + e_{bs2}(t) \tag{2.5}$$

The voltage, $e_{bs1}(t)$, introduced due to mechanical motion of the speaker cone is linearly proportional to the speaker cone velocity, v_{spkr}

$$e_{bs1}(t) = (bl)v_{spkr}(t) \tag{2.6}$$

The voltage, $e_{bs2}(t)$, in the secondary speaker coil can be written from the constitutive relation (2.1) of the coils by noting that the secondary coil current, $i_s = 0$ due to the open circuit on secondary coil.

$$e_{bs2}(t) = \dot{\lambda}_s = M_{coil}\frac{di_p(t)}{dt} \tag{2.7}$$

Hence, the voltage, $e_{bs}(t)$, introduced in secondary speaker coil is

$$e_{bs}(t) = (bl)v_{spkr} + M_{coil}\frac{di_p}{dt} \tag{2.8}$$

Equations (2.4) and (2.8) define the model of a dual-wound coil subwoofer speaker. The speaker parameters necessary to define the model are: mechanical inertia of speaker, I_{spkr}, mechanical compliance of speaker, C_{spkr}, viscous friction of speaker, R_{spkr}, electromagnetic coupling factor, (bl), speaker coil resistance, R_{coil}, speaker coil inductance, I_{coil}, mutual inductance, M_{coil}, and the equivalent speaker area , S_D. With the exception of mutual inductance, M_{coil}, these electrical and mechanical parameters are defined in IEEE standard 219-1975 for loudspeaker measurements.

2.3. Speaker Transfer Functions

The transfer functions of the subwoofer speaker system describe the dynamics between mechanical and electrical subsystems of the speaker. One of these transfer functions is the plant transfer function, $G_{spkr}(s)$, from the primary coil drive voltage, $e(t)$, to the speaker cone velocity, v_{spkr}. The other transfer function describes the dynamics between speaker cone velocity, v_{spkr}, and the voltage, $e_{bs}(t)$, introduced in the secondary speaker coil . Denoted $H_1(s)$, this transfer function was the basis for speaker cone velocity sensor design. The knowledge of both transfer functions is important to speaker velocity feedback compensator design.

The plant transfer function, $G_{spkr}(s)$, between drive voltage and speaker cone velocity can be written from (2.4) by noting that volumetric flow rate, $Q(t)$ is equal to speaker cone velocity, v_{spkr}, times its effective area, S_D.

$$G_{spkr}(s) = \frac{(bl)/I_{coil}\ \ s}{I_{spkr}s^3 + (R_{spkr} + \frac{R_{coil}I_{spkr}}{I_{coil}})s^2 + (\frac{1}{C_{spkr}} + \frac{R_{coil}R_{spkr} + (bl)^2}{I_{coil}})s + \frac{R_{coil}}{I_{coil}C_{spkr}}} \tag{2.9}$$

The transfer function, $H_1(s)$, between speaker cone velocity, v_{spkr}, and secondary coil voltage, e_{bs}, is obtained by taking the Laplace transform of (2.8)

$$\frac{E_{bs}(s)}{V_{spkr}(s)} = (bl) + s\frac{M_{coil}I_p(s)}{V_{spkr}(s)} \tag{2.10}$$

The transfer function between primary coil current, i_p, and speaker cone velocity, v_{spkr}, can be written from (2.4) as

$$\frac{I_p(s)}{V_{spkr}(s)} = \frac{I_{spkr}s^2 + R_{spkr}s + 1/C_{spkr}}{(bl)s} \tag{2.11}$$

From (2.10) and (2.11)

$$H_1(s) = \frac{E_{bs}(s)}{V_{spkr}(s)} = \frac{M_{coil}}{(bl)}(I_{spkr}s^2 + R_{spkr}s + (1/C_{spkr} + (bl)^2/M_{coil})) \tag{2.12}$$

Transfer functions (2.9) and (2.12) are the speaker transfer functions required for sensor and speaker compensation.

2.4 Speaker Parameter Identification Procedure

Parameter identification for the speaker model is based upon the structure of the model equations. Experimental tests to identify the speaker parameters neglect the coil inductance, I_{coil}. Below 200 Hz, the electric time constant determined by coil inductance and coil resistance is small compared to the mechanical time constant. This allows neglecting the speaker coil inductance and reduces the speaker transfer function (2.9) to a second order form

$$\frac{V_{spkr}(s)}{E(s)} = \frac{(bl)/(I_{spkr} \times R_{coil})\ s}{s^2 + 2\zeta\omega_n s + \omega_n^2} \tag{2.13}$$

where:

$$\omega_n^2 = \frac{1}{C_{spkr} I_{spkr}} \tag{2.14}$$

and

$$\zeta = \frac{1}{2}\sqrt{\frac{C_{spkr}}{I_{spkr}}}\left(R_{spkr} + \frac{(bl)^2}{R_{coil}}\right) \tag{2.15}$$

The speaker mechanical compliance, C_{spkr}, can be independently measured from speaker diaphragm displacement, x_{spkr}, for a known force, F, using force and displacement measurements.

$$C_{spkr} = \frac{x_{spkr}}{F} \tag{2.16}$$

The speaker mechanical inertia , I_{spkr}, is obtained from (2.14).

$$I_{spkr} = \frac{1}{C_{spkr} \times \omega_n^2} \quad \text{where } \omega_n = 2\pi f_n \tag{2.17}$$

The fundamental natural frequency, f_n, is the frequency at which the velocity response phase passes through 0 degrees since the velocity frequency response starts with a 90^o phase lead and is obtained from experimental speaker cone phase response (Figure 2.5). The fundamental natural frequency, f_n, is independent of the damping ratio, ζ. The damping ratio, ζ, is obtained from the quality factor, Q.

$$\zeta = \frac{1}{2Q} \tag{2.18}$$

Quality factor, Q, is determined from the half power points on the experimental speaker cone velocity magnitude response (Figure 2.5) following the IEEE standard 219-1975 for loudspeaker measurements.

$$Q = \frac{f_n}{f_2 - f_1} \tag{2.19}$$

Frequencies f_1 and f_2, are the frequencies at which the velocity of speaker falls to 0.707 (-3 dB) of its value at resonance. The electromagnetic coupling factor, (bl), can be obtained from the experimental speaker cone velocity frequency response. Let the log-magnitude of the response at frequency ω_1(rad/sec) be M. From (2.13), the log-magnitude, M, of speaker cone velocity response at frequency ω_1 is given by

$$M = 20\log_{10} \frac{\sqrt{[bl \times \omega_1(\omega_n^2 - \omega_1^2)]^2 + [2 \times bl \times \zeta\omega_1^2\omega_n]^2}}{I_{spkr} \times R_{coil} \times [(\omega_n^2 - \omega_1^2)^2 + (4\zeta^2\omega_1^2\omega_n^2)]} \tag{2.20}$$

Using (2.20), it is possible to determine the value of (bl). Viscous friction, R_{spkr}, is obtained from (2.15) and (2.18).

$$R_{spkr} = \frac{\sqrt{I_{spkr}}}{Q\sqrt{C_{spkr}}} - \frac{(bl)^2}{R_{coil}} \tag{2.21}$$

The speaker coil resistance, R_{coil}, in (2.21) is measured with an ohmmeter. The equivalent speaker cone area, S_D, is taken as 87% of the speaker cone area computed from nominal speaker diameter to account for the area taken by the flexible cone connection to the speaker frame (Beranek, 1986).

2.5. Parameter Identification of a Dual-Wound Coil Subwoofer Speaker

The laboratory procedure described in previous section for identifying the speaker parameters was validated using a dual-coil subwoofer speaker for which no parameters were available. The velocity frequency response was measured by a Brüel & Kjaer Laser Doppler Velocity-transducer Set Type 3544 (Figure 2.4). The Doppler Frequency shift in the target beam caused by the vibration of the speaker cone was detected and converted into a calibrated voltage output proportional to the cone velocity. A Hewlett Packard Dynamic Signal Analyzer 35660A was used to obtain the frequency response of the transfer function between speaker cone velocity and the input drive voltage to the speaker. Fundamental natural frequency, $f_n = 21$ Hz and quality factor, $Q = 0.3944$ were obtained from the experimental speaker cone velocity frequency responses (Figure 2.5). The computed speaker parameters from the experimental measurements are tabulated in Table 1.1.

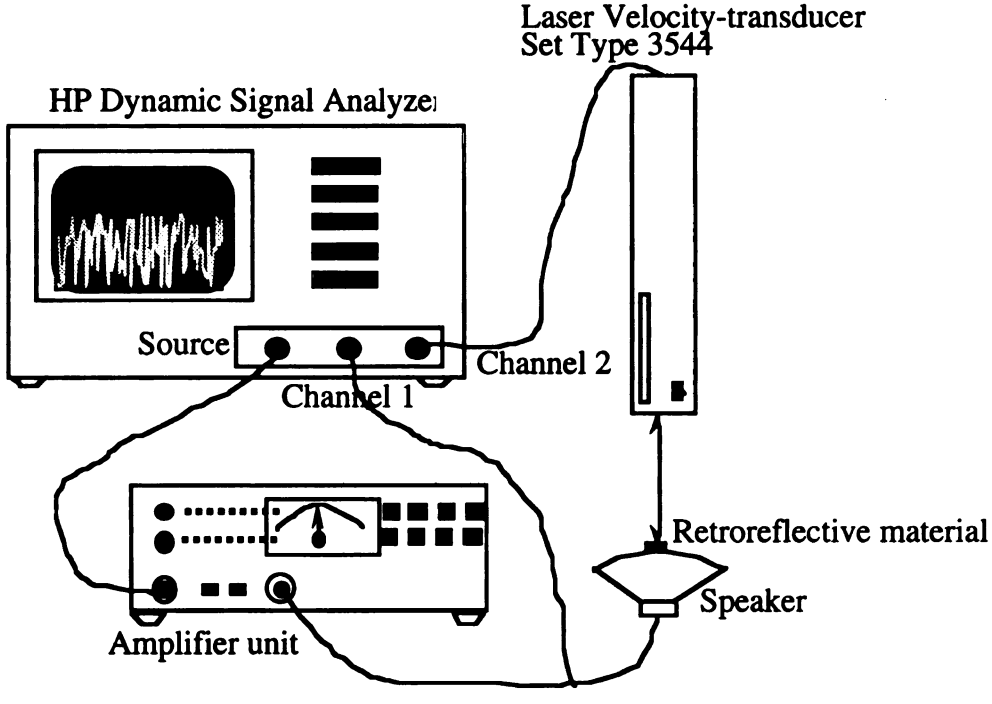

Figure 2.4. Schematic of Experimental Setup for Measuring Speaker Velocity Response

Table 1.1 Identified Parameters for a Dual-Wound Subwoofer Speaker

Parameter	Value
Mechanical Inertia , I_{spkr}	55.5 gm
Mechanical Compliance, C_{spkr}	1.03 mm/N
Viscous Friction, R_{spkr}	7.8 N-sec/m
Electromagnetic Coupling Factor, (bl)	5.4 N/A
Coil Resistance, R_{coil}	3.5 Ohms
Coil Inductance, I_{coil}	2.8 mH
Equivalent Speaker Area , S_D	531 cm^2

A analytical model (2.13) of the subwoofer speaker without speaker coil inductance was then constructed and simulated in MatLab® using the parameters in Table 1.1. The model and measured frequency responses are shown in Figure 2.5 and have the same fundamental natural frequency, $f_n = 21$ Hz, indicated by phase response zero crossings. At 300 Hz, the measured velocity response magnitude is 25 dB below its value at 21 Hz resonance. This makes the effect of noise dominant above 300 Hz and accordingly measurements above 300 Hz were found unreliable due to poor signal-to noise ratio. The model and measured responses agree well up to approximately 200 Hz. After 200 Hz, the difference between model and measured frequency responses is attributed to the effect of speaker coil inductance neglected in the speaker model (2.13).

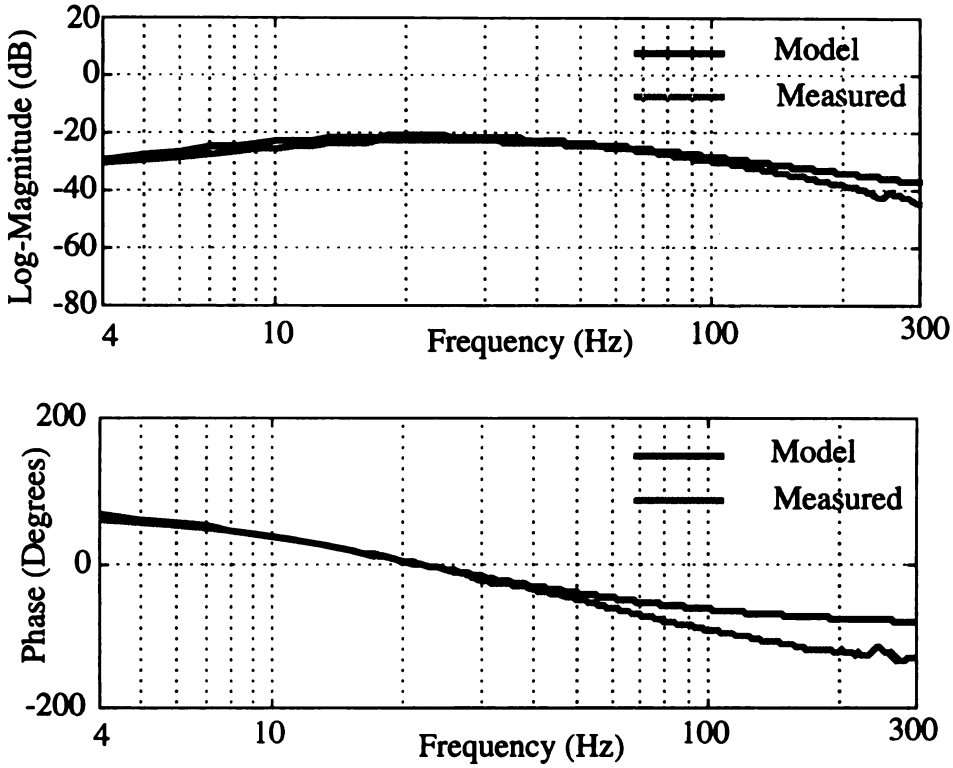

Figure 2.5. Comparison of Measured and Speaker Model Velocity Responses without Speaker Coil Inductance (dB re 1)

The analytical model (2.9) of the subwoofer model with speaker coil inductance was constructed and simulated in MatLab®. A speaker coil inductance of 2.8 mH was used to obtain a good fit between the model and measured responses (Figure 2.6). The close agreement between the model and measured responses indicate that the presence of speaker coil inductance in the speaker model is essential.

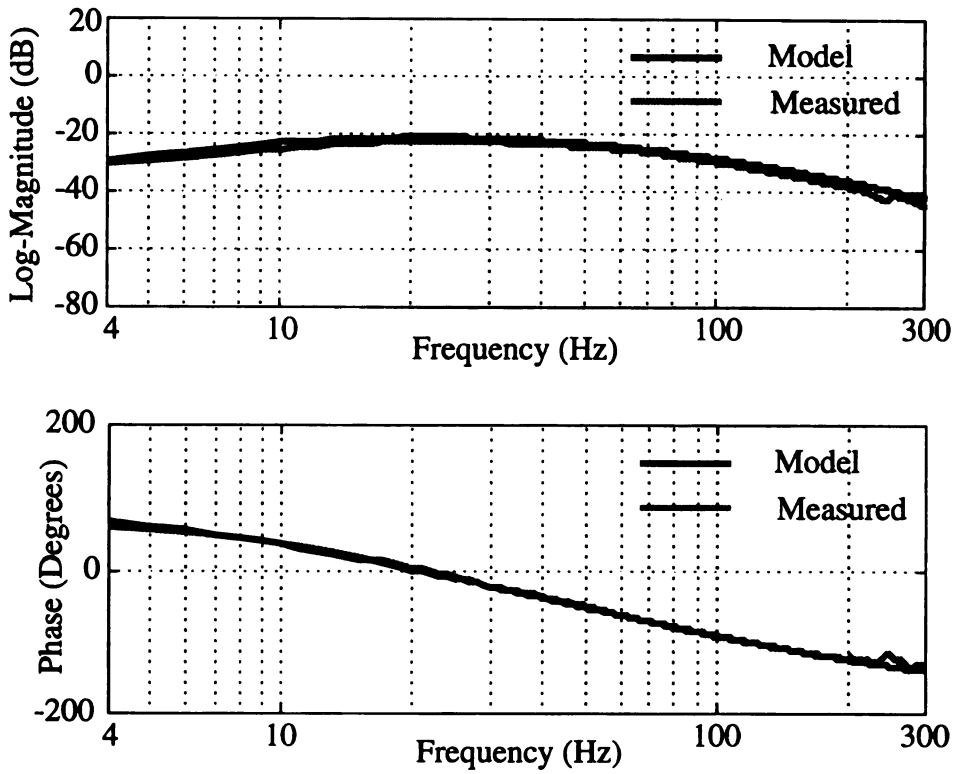

Figure 2.6. Comparison of Measured and Speaker Model Velocity Responses with Speaker Coil Inductance (dB re 1)

2.6. Speaker Enclosure Effects

The enclosure which supports the speaker drive unit has an acoustical effect of increasing the speaker free air resonance. This effect is represented by acoustic compliance, C_{box}, and acoustic resistance, R_{box}. in the bond graph model of speaker (Figure 2.7). The acoustic pressure inside the speaker enclosure is denoted by $P_{int}(t)$ while $P(t)$ represents the speaker face acoustic pressure. The speaker drive voltage, $e(t)$, and the speaker face pressure, $P(t)$ form the two inputs for the speaker system. The acoustic compliance, C_{box}, models the flexibility of air inside the enclosure and is given by (Beranek, 1986)

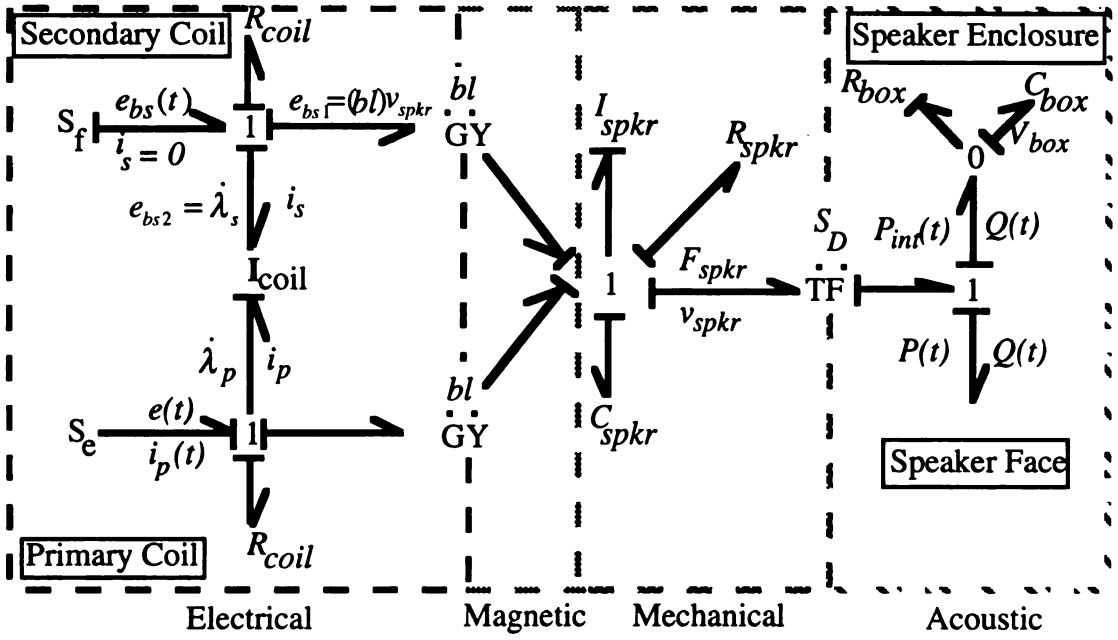

Figure 2.7. Bond Graph Model of Dual-Wound Coil Subwoofer Speaker with Enclosure

$$C_{box} = \frac{V_{box}}{\rho_{air} c_{air}^2} \tag{2.22}$$

where, V_{box} is the volume of speaker enclosure. The volume of the speaker is subtracted from the actual volume of enclosure in order to obtain V_{box}. As a first approximation, the volume of speaker in meters^3 equals 0.4 times the fourth power of the advertised diameter in meters (Beranek, 1986). The acoustic resistance, R_{box}, models the pressure drop associated with the leakage in the speaker enclosure.

The state-space equations for the speaker with enclosure can be written by selecting energy variables : speaker cone displacement, x_{spkr}, speaker cone velocity, v_{spkr}, primary coil flux linkage, λ_p, and volume displacement, V_{box} as state variables. The input variables for the state-space model are speaker drive, $e(t)$, and speaker face pressure, $P(t)$ while the output variables are speaker volumetric flow rate, $Q(t)$ and primary coil current, $i_p(t)$.

$$\frac{d}{dt}\begin{pmatrix} x_{spkr} \\ v_{spkr} \\ \lambda_p \\ V_{box} \end{pmatrix} = \begin{bmatrix} 0 & 1 & 0 & 0 \\ \frac{-1}{C_{spkr}I_{spkr}} & \frac{-R_{spkr}}{I_{spkr}} & \frac{bl}{(I_{spkr}I_{coil})} & \frac{-S_D}{C_{encl}} \\ 0 & -bl & \frac{-R_{coil}}{I_{coil}} & 0 \\ 0 & S_D & 0 & \frac{-1}{R_{box}C_{box}} \end{bmatrix} \begin{pmatrix} x_{spkr} \\ v_{spkr} \\ \lambda_p \\ V_{box} \end{pmatrix} + \begin{bmatrix} 0 & 0 \\ 0 & \frac{-S_D}{I_{spkr}} \\ 1 & 0 \\ 0 & 0 \end{bmatrix} \begin{pmatrix} e(t) \\ P(t) \end{pmatrix} \tag{2.23a}$$

$$\begin{pmatrix} Q(t) \\ i_p(t) \end{pmatrix} = \begin{bmatrix} 0 & S_D & 0 & 0 \\ 0 & 0 & \frac{1}{I_{coil}} & 0 \end{bmatrix} \begin{pmatrix} x_{spkr} \\ v_{spkr} \\ \lambda_p \\ V_{box} \end{pmatrix} \tag{2.23b}$$

This state-space equation is similar to (2.4) with an additional state, V_{box}, corresponding to the volume of the speaker enclosure.

Enclosure effect was verified on the dual-wound coil subwoofer speaker for which parameters are given in Table 1.1. The speaker was placed in a rectangular enclosure of dimensions 35 cm × 24 cm × 55 cm. From (2.22), the acoustic compliance of the enclosure is $C_{encl} = 3.25 \times 10^{-7}$ m^3/Pa. The analytical model of the enclosed speaker from input voltage, $e(t)$ to speaker cone velocity, v_{spkr} was obtained from (2.23) and simulated in MatLab®. An acoustic resistance of 2.78×10^4 Pa-sec/m^3 was used to obtain a good fit between the model and measured responses (Figure 2.8). The measured and model responses have the same fundamental natural frequency, $f_n = 65$ Hz, shown by phase response zero crossings. The enclosure thus has the effect of increasing speaker free-air resonance. At frequencies above 300 Hz, the model response diverges from the measured response. This effect can be attributed to the standing wave acoustic modes of the speaker enclosure. The first acoustic mode along 55 cm direction of the speaker enclosure occurs at 313 Hz. It has an influence on the magnitude and phase responses at frequencies below 313 Hz and affects the low-frequency speaker behavior.

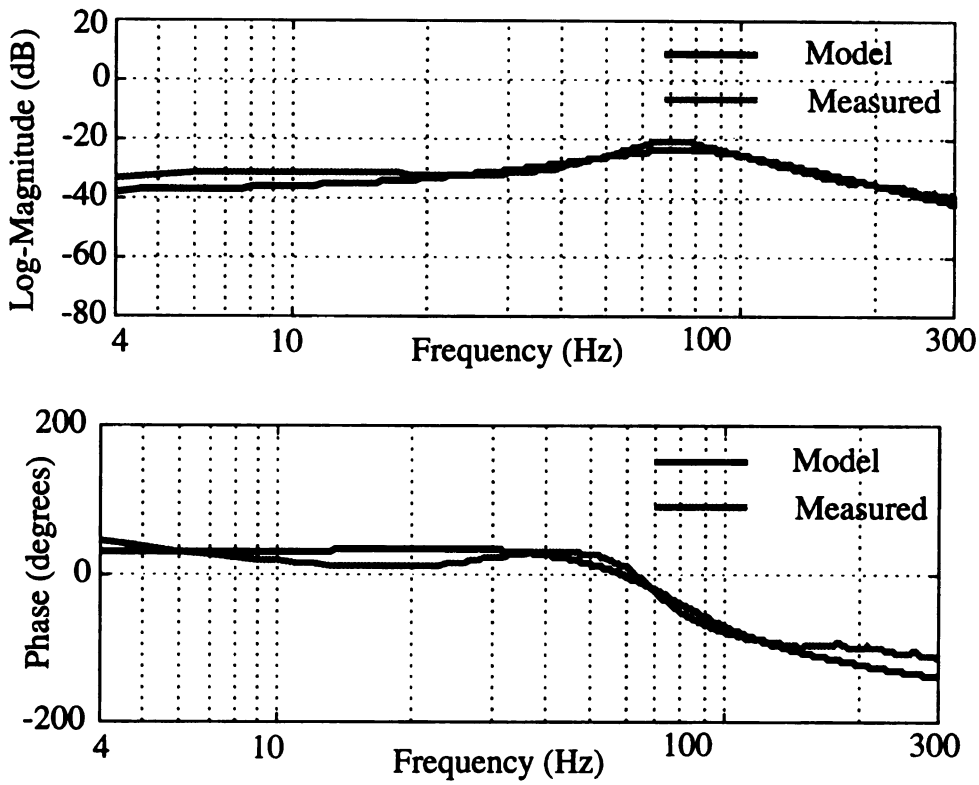

Figure 2.8. Comparison of Measured and Enclosed Speaker Model Velocity Response (dB re 1)

The velocity frequency responses shown in Figure 2.8 have limited bandwidth and large phase shifts that prevents speaker cone velocity tracking of desired velocity inputs. This makes it an unsuitable actuator in AAS where speaker cone velocity must track the speaker face pressure with minimum magnitude and phase variation. These bandwidth limited speakers are unsuitable acoustic control actuators unless compensation is provided for their varying velocity response.

2.7. Summary

A simple laboratory based methodology for identifying speaker dynamics for acoustic control applications has been presented and experimentally validated in

laboratory tests on a dual-wound coil subwoofer speaker. The analytical model response was found to agree well with the measured response. The effects of speaker enclosure was also discussed. The enclosure was shown to increases the speaker free air resonance.

The speaker velocity response has limited bandwidth and large phase variations. These magnitude and phase variations make speakers ineffective control actuators for acoustic system where input is proportional to actuator input velocity. Compensation for the varying velocity response of speakers is needed to make them effective acoustic control actuators.

Chapter 3 Velocity Feedback Compensation of Speakers

3.1. Introduction

Electromechanical speakers commonly used as control actuators in acoustic applications have a non-constant voltage-to-velocity frequency response due to the free-air resonance of the speaker (Figures 2.6 and 2.8). Speaker volumetric flow rate cannot accurately follow the controller output signals if the variations in velocity frequency response occur within the acoustic control system bandwidth. This makes electromechanical speakers ineffective as control actuators unless a compensation is provided for their varying velocity response.

The idea of compensating speaker velocity response dates back to early 1920s. Articles on this subject (Harwood, 1974, Klaassen, et al., 1968, Holdaway, 1963, Werner, 1958, Holle, 1952, Tanner, 1951) mention the use of velocity feedback as the compensation technique. They, however, differ on the method used for sensing speaker cone velocity. The earliest mention of speaker compensation is found in a patent (no. 231972) awarded to P. G. A. H. Voigt on Jan. 29th 1924. In his patent, Voigt used back emf induced in the speaker coil by its motion in the magnetic field as a measure of speaker cone velocity. The difficulties reported in his implementation (Harwood, 1974) were the needs to compensate for temperature induced changes in speaker coil resistance and frequency dependent variations in speaker coil inductance. Another speaker compensation is found in a patent (no. 272622) by A. F. Sykes dated March 20th 1926. He used voltage introduced in an auxiliary coil to sense the speaker cone velocity. The method was not successful because the mutual inductance between auxiliary and speaker coil introduced

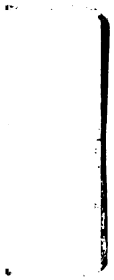

errors in the speaker cone velocity sensing. In a third implementation, M. Trouton in his patent (no. 320713, Aug. 10th 1928) used the voltage obtained from speaker cone displacement in a capacitive method to sense speaker cone velocity. The method though relatively simple, required a considerable spacing between capacitive elements for large amplitudes motions of speaker cone. Non-axial movement of the speaker coil also introduced error in this method. The use of accelerometers to measure speaker cone velocity has also been mentioned (Klaassen et al., 1968). In this method, the output of accelerometer attached to the speaker cone diaphragm is integrated to obtain voltage proportional to speaker cone velocity. The obvious disadvantages in this method are the inaccuracies in integrator due to noise and accelerometer mass loading of the speaker cone. The novel speaker cone velocity sensor developed in this work uses the mutual inductance effect compensated voltage introduced in an auxiliary speaker coil. The compensated auxiliary coil voltage provides an accurate velocity sensor and does not have the problems associated with sensors mentioned above.

3.2. Speaker Velocity Feedback Design

Velocity feedback compensation (Figure 3.1) for minimizing the magnitude and phase variations in speaker velocity response is designed and demonstrated in laboratory tests on a dual-wound coil subwoofer speaker. The feedback compensation uses proportional controller, K_p to generate drive voltage, $e(t)$ at the primary set of speaker coils. The speaker cone velocity is obtained through sensor transfer function, $H(s)$. The closed loop system transfer function, $T(s)$, from block diagram (Figure 3.1) is

$$T_{spkr}(s) = \frac{V_{spkr}(s)}{V_d(s)} = \frac{K_p G_{spkr}(s)}{1 + K_p G_{spkr}(s) H(s)} \tag{3.1}$$

where, $V_d(s)$ is the Laplace transform of desired velocity input, $v_d(t)$. $G_{spkr}(s)$ is the open-loop transfer function of enclosed subwoofer speaker. As the proportional compensator gain, K_p, is increased, the closed loop transfer function approaches $1/H(s)$. If the sensor transfer function is a real constant, β, over the controller bandwidth, ω_b,

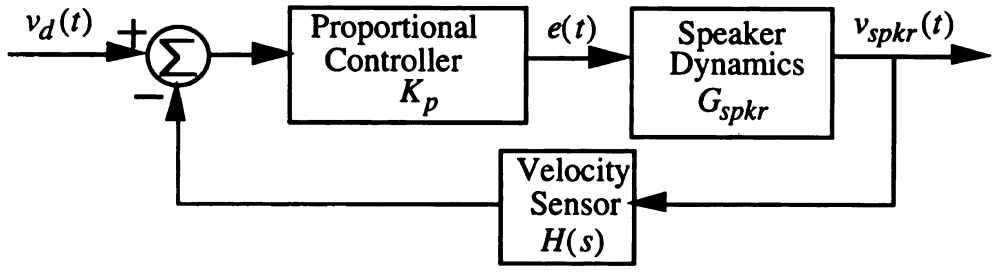

Figure 3.1. Schematic of Speaker Velocity Feedback Compensation

$$H(j\omega) = \beta \quad \forall\ \omega \in [0, \omega_b] \tag{3.2}$$

the closed loop transfer function, $T_{spkr}(s)$, will approach a constant, $1/\beta$, with zero phase. This compensation forces speaker cone velocity to accurately follow the desired velocity input. The result is independent of the speaker dynamics provided the sensor has a constant transfer function (3.2) over the controller bandwidth. Proper selection and design of the velocity sensor is critical.

3.3. Speaker Cone Velocity Sensor Design

An accurate speaker cone velocity sensor is necessary for the successful performance of closed loop speaker velocity feedback system. A novel cone velocity sensor design for a dual-wound coil subwoofer speaker is discussed here. It uses speaker cone velocity induced voltage in a secondary speaker coil obtained by compensating the mutual inductance effect between dual-wound coils.

The transfer function from speaker cone velocity to secondary speaker coil voltage for the enclosed dual-wound coil subwoofer can be obtained from the state-space equation for the enclosed speaker. The voltage, $e_{bs}(t)$, introduced in secondary speaker coil is given by (2.8).

$$e_{bs}(t) = (bl)v_{spkr} + M_{coil}\frac{di_p}{dt} \tag{3.3}$$

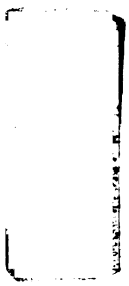

The transfer function, $H_1(s)$, between speaker cone velocity and secondary coil voltage is obtained by taking Laplace transform of (3.3)

$$\frac{E_{bs}(s)}{V_{spkr}(s)} = (bl) + s\frac{M_{coil}I_p(s)}{V_{spkr}(s)} \tag{3.4}$$

The right hand side of (3.4) can be manipulated using the following Laplace domain equation obtained from (2.22).

$$V_{box}(s) = \frac{S_D}{s + (1/R_{box}C_{box})}V_{spkr}(s) \tag{3.5}$$

$$(s^2 + \frac{R_{spkr}}{I_{spkr}}s + \frac{1}{C_{spkr}I_{spkr}})V_{spkr}(s) = \frac{(bl)s}{I_{spkr}}I_p(s) - \frac{S_D \times s}{C_{box}I_{spkr}}V_{box}(s) \tag{3.6}$$

From Equations (3.5) and (3.6)

$$(s^2 + \frac{R_{spkr}}{I_{spkr}}s + \frac{1}{C_{spkr}I_{spkr}})V_{spkr}(s) = \frac{(bl)s}{I_{spkr}}I_p(s) - \left[1 - \frac{1}{(R_{box}C_{box})s+1}\right]\frac{S_D^2 V_{spkr}(s)}{C_{box}I_{spkr}} \tag{3.7}$$

From (3.4) and (3.7), the transfer function, $H_1(s)$, between speaker cone velocity and secondary coil voltage can be written as

$$H_1(s) = \frac{E_{bs}(s)}{V_{spkr}(s)} = \frac{M_{coil}\left[As^3 + Bs^2 + Cs + D\right]}{(bl) \times (R_{box}C_{box}s + 1)} \tag{3.8}$$

where, $A = \left(R_{box}I_{spkr}C_{box}\right)$; $B = \left(I_{spkr} + R_{box}R_{spkr}C_{box}\right)$

$$C = \left(R_{spkr} + \frac{R_{box}C_{box}}{C_{spkr}} + S_D^2 R_{box} + \frac{R_{box}(bl)^2 C_{box}}{M_{coil}}\right); \quad D = \left(\frac{M_{coil} + (bl)^2}{M_{coil}C_{spkr}}\right)$$

One of the zeros of the transfer function $H_1(s)$ can be approximated by $(R_{box}C_{box}s + 1)$. This reduces $H_1(s)$ to a complex second order zero. The validity of this assumption is verified later in computer simulations.

$$H_1(s) = \frac{M_{coil}}{(bl)}\left[I_{spkr}s^2 + R_{spkr}s + \left(\frac{1}{C_{eq}} + \frac{(bl)^2}{M_{coil}}\right)\right] \tag{3.9}$$

where

$$C_{eq} = \frac{C_{box} C_{spkr}}{C_{box} + S_D^2 C_{spkr}} \tag{3.10}$$

is defined as the equivalent speaker compliance due to speaker mechanical compliance, C_{spkr}, and the enclosure acoustic compliance, C_{box}.

The measured and analytical frequency responses of the transfer functions (3.8) and (3.9) for the dual-wound coil subwoofer speaker (Table 1.1) placed in an enclosure of dimensions 35 cm × 24 cm × 55 cm are shown in Figure 3.2. From section 2.6, the enclosure acoustic compliance, $C_{encl} = 3.25 \times 10^{-7}$ m^3/Pa. This gives an equivalent speaker compliance of 0.104 mm/N. The analytical frequency responses are obtained by simulating the transfer functions (3.8) and (3.9) with an equivalent speaker compliance of 0.104 mm/N while other speaker parameters are obtained from Table 1.1. The mutual inductance, M_{coil}, was not supplied by the speaker manufacturer and a value of 1.2 mH provided a good fit between model and measured responses. A Hewlett Packard Dynamic Signal Analyzer 35660A was used to measure the frequency response between speaker cone velocity and secondary speaker coil voltage. The measured frequency response agrees well with the analytical model responses over 4-300 Hz bandwidth. The close agreement between the second (3.9) and third order model (3.8) responses justifies the pole-zero cancellation of $(R_{box} C_{box} s + 1)$ in (3.8). It allows the transfer function, $H_1(s)$, to be represented by a damped second order zero ($\zeta = 0.24$) at 122 Hz (3.9) as indicated by 90° phase crossing (Figure 3.2).

The secondary speaker coil voltage due to mechanical motion of speaker cone is linearly proportional (2.6) to the speaker cone velocity through electromagnetic coupling factor, (bl). It provides a good measure of speaker cone velocity below 70 Hz as seen from Figure 3.2. Over this frequency range, the phase is nearly 0° and the magnitude varies from 13.5 dB to 14.8 dB which is the electromagnetic coupling factor, (bl). At frequencies above 70 Hz, the second order zero at 122 Hz due to mutual inductance

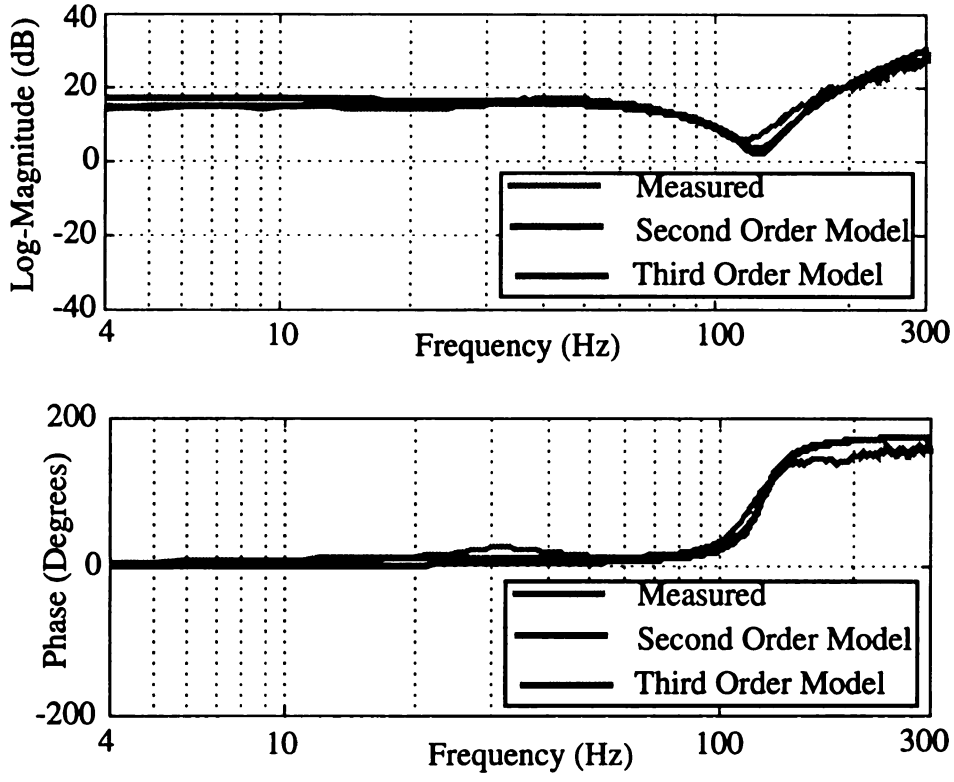

Figure 3.2. Secondary Coil Voltage/Speaker Cone Velocity Model vs. Measured Responses (dB re 1)

between the dual-wound coils causes large magnitude and phase changes. The secondary speaker coil voltage becomes an inaccurate velocity sensor above 70 Hz unless the sensor is compensated for the second order zero at 122 Hz. A second order filter, $H_c(s)$, with an undamped natural frequency of 122 Hz and a damping ratio of $\zeta = 0.24$ was built to compensate for this mutual inductance zero.

The mutual inductance compensated frequency response between speaker cone velocity and secondary speaker coil voltage has less than 5 dB gain variation over 4-300 Hz (Figure 3.3) frequency range compared to 30 dB variation for uncompensated secondary coil voltage (Figure 3.2). Over the same range of frequencies, phase varies less

than 20° for filtered secondary coil voltage compared to a variation of 160° for uncompensated secondary coil voltage. Although some magnitude and phase variations remain, the filtered secondary speaker coil voltage provides a more accurate measure of speaker cone velocity. It provides a speaker cone velocity sensor whose transfer function, $H(s)$, can be assumed to be unity with zero phase over 4-300 Hz frequency range.

This velocity sensor does not have the drawbacks of previously mentioned sensors. There is no need to account for the temperature induced variations in speaker coil resistance and frequency dependent variations in speaker coil inductance as in Voigt's method. The sensor does not mechanically load the speaker cone as in the velocity

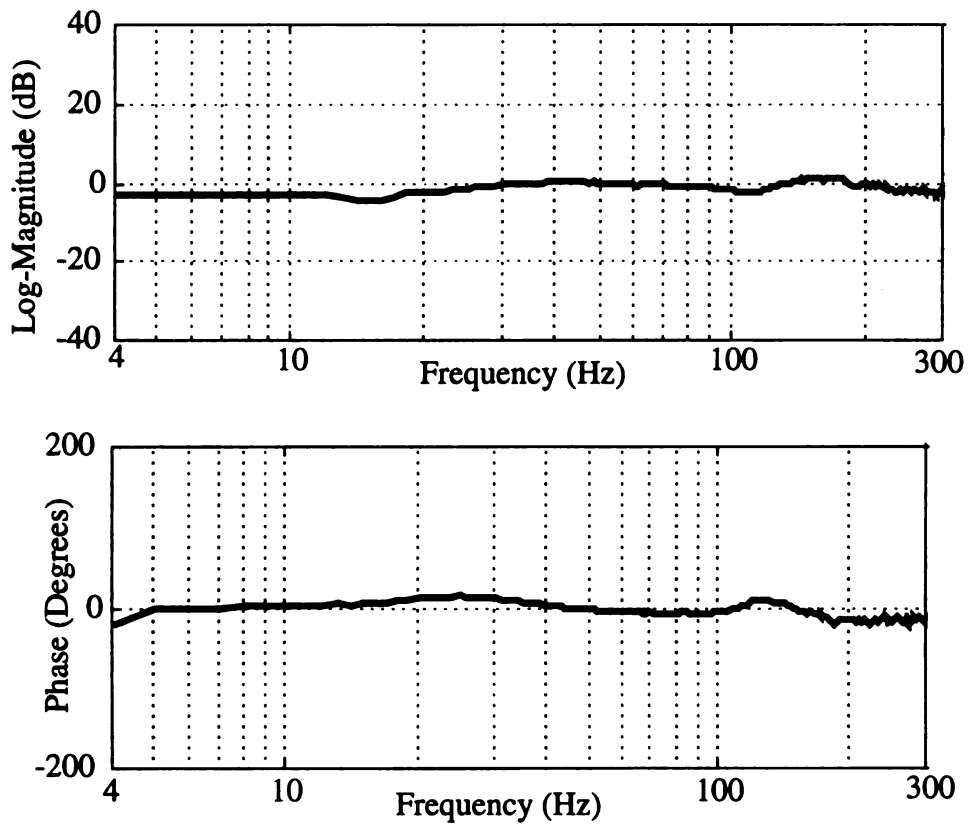

Figure 3.3. Compensated Secondary Speaker Coil Voltage/Laser Velocity Response (dB re 1)

sensors using accelerometers. There are no geometric inaccuracies associated with using capacitive pick-up elements. This unique velocity sensing mechanism requires only the filter and does not need any changes in the physical parameters of the subwoofer speaker. It yields a viable velocity sensor for the feedback compensation of the speaker system.

3.4 Stability Analysis of Speaker Velocity Feedback System

A closed loop stability analysis of the speaker velocity feedback system determines the maximum stable gain of the proportional controller (Figure 3.1). The closed loop system transfer function, $T_{spkr}(s)$, is given by (3.1) where, $K_p G_{spkr}(s)H(s)$ is the open-loop transfer function. The maximum stable gain, $K_{p,max}$ of the proportional controller is given by the gain margin, GM, of system open-loop transfer function.

$$K_{p,max} = GM = \frac{1}{\left|K_p G_{spkr}(j\omega_1)H(j\omega_1)\right|} \tag{3.11}$$

where, ω_1, the phase crossover frequency, is the frequency at which the phase angle of the open-loop transfer function becomes -180^0. The gain margin can be evaluated from the bode diagram which is a plot of magnitude and phase of open-loop transfer function versus frequency.

The bode plot of the speaker velocity feedback system (Figure 3.1) for $K_p = 1$ was experimentally measured (Figure 3.4) over 4-300 Hz frequency range. The measured phase response does not cross -180° over 4-300 Hz indicating that the closed loop speaker system will be stable with infinite gain margin. It must be noted that the phase response will eventually cross -180° at some frequency above 300 Hz due to the minimum phase nature of the open-loop transfer function of the enclosed speaker. This will reduce the gain margin and thereby limit the gain of the proportional controller. The 20 dB/decade roll off in the magnitude response, however, will provide enough gain margin at the phase crossover frequency above 300 Hz before destabilizing the closed-loop system. This fact was verified by plotting an analytical root locus plot of the speaker system.

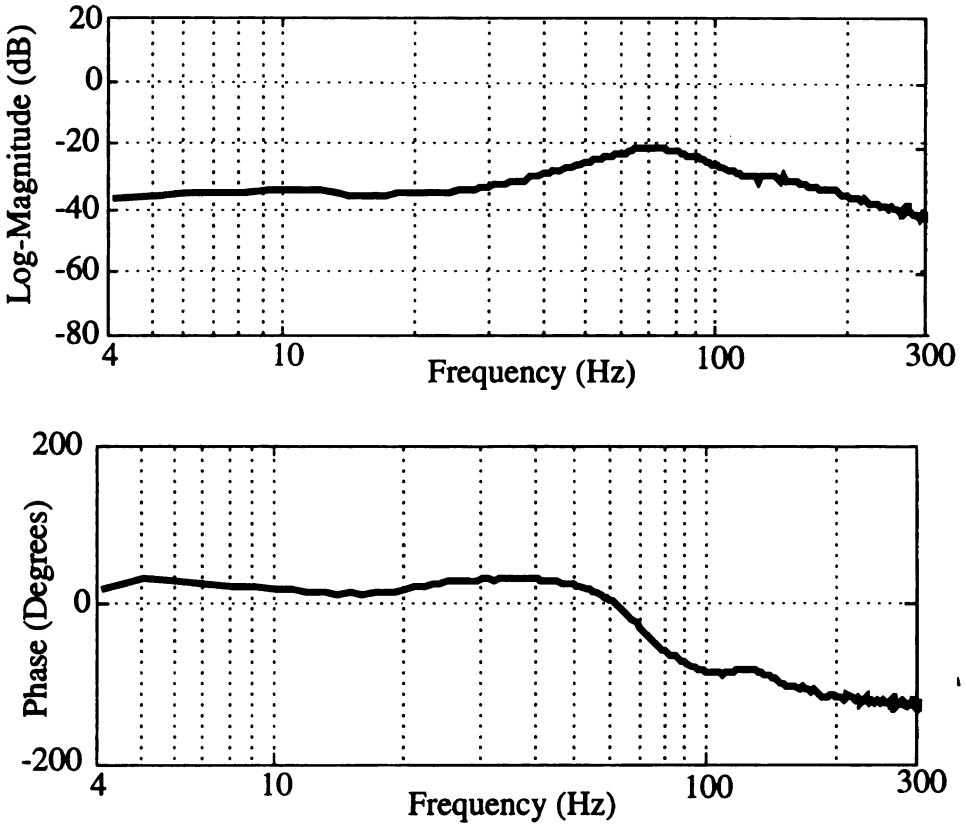

Figure 3.3. Measured Bode Plot of the Open-Loop Transfer Function of Speaker Velocity Feedback System (dB re 1)

A root locus of the closed-loop speaker velocity feedback system (Figure 3.1) using an analytical model of enclosed speaker (2.22) is shown in Figure 3.5. The velocity sensor transfer function is assumed to be unity with zero phase (Figure 3.3). The root locus is plotted by varying the proportional controller gain, K_p, from 0 to 110 and indicates the location of closed-loop poles in complex plane as a function of K_p. It is clear from the root locus that closed-loop poles lie in the left-half complex plane indicating a stable closed-loop system. The limiting value of the proportional controller gain at which one of the closed-loop poles becomes zero is found from the Routh-Hurwitz criteria to be 10^5. The closed-loop system thus becomes marginally stable at a

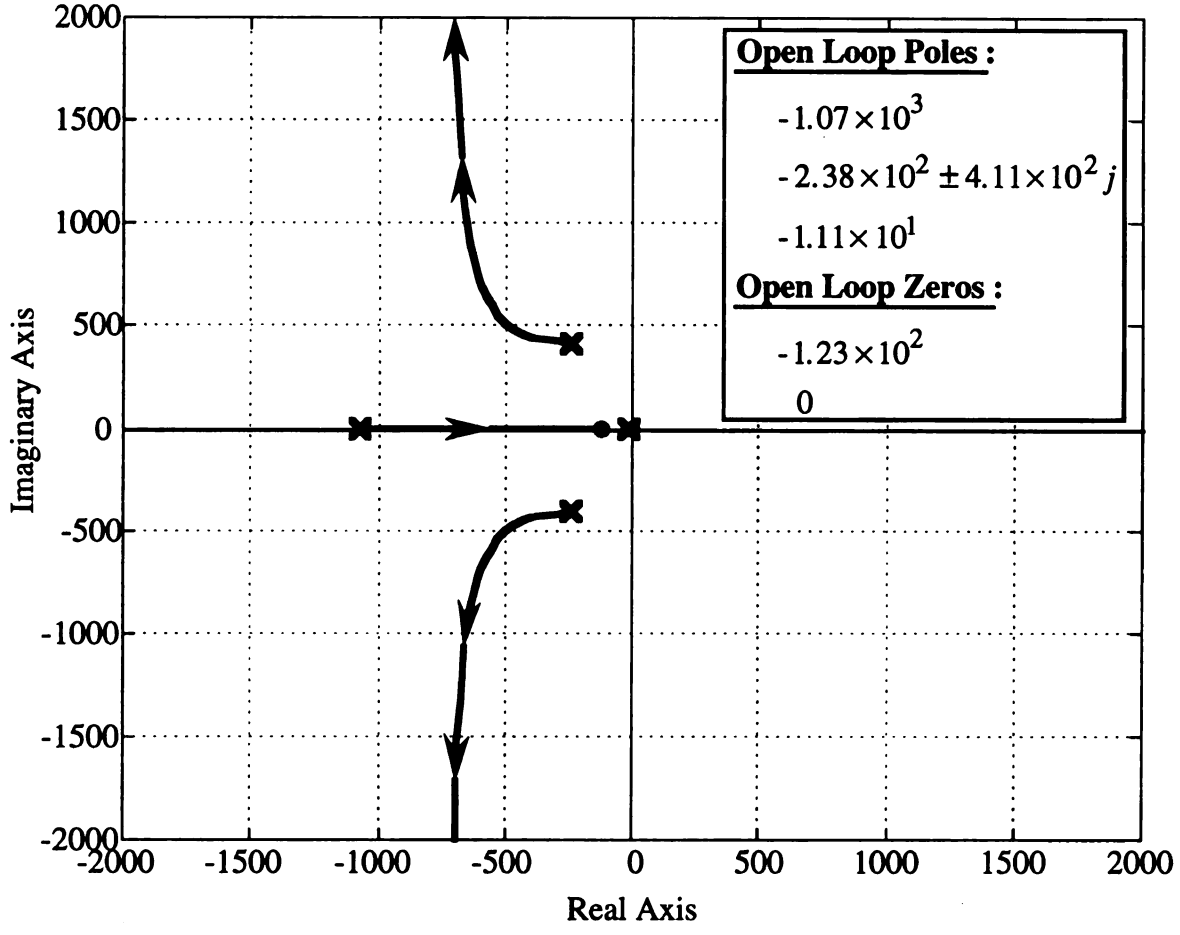

Figure 3.5. Root Locus of Velocity Feedback System for Varying Proportional Controller Gain

proportional gain of 10^5. This indicates an almost infinite gain margin and this was expected from the experimental results shown earlier. It is thus possible to implement the velocity feedback controller over a low frequency bandwidth without destabilizing the closed-loop system.

3.5. Performance Evaluation of Speaker Velocity Feedback

The performance of the speaker velocity feedback compensator was evaluated by measuring (Figure 3.6) the closed loop transfer function, $T_{spkr}(s)$, of the speaker velocity

feedback loop (Figure 3.1) for different proportional compensator gains (Figures 3.7-3.10). The speaker cone velocity was independently measured using laser velocimeter. As the proportional compensator gain is increased, the magnitude of the closed loop speaker velocity response becomes more constant and phase change is minimized. At a compensator gain of $K_p = 200$, the magnitude varies less than 5 dB from 4 Hz to 300 Hz as compared to an open loop magnitude change of 20 dB. Over this range of frequencies, the phase angle changes less than 20 degrees as compared to an open loop change of 160 degrees. At high proportional gains, the closed loop transfer function (Figure 3.10) approaches the inverse (3.2) of the sensor transfer function, $H(s)$ as expected (3.1). When compared to the uncompensated speaker, the feedback compensated subwoofer speaker has much lower magnitude and phase variations in the velocity response.

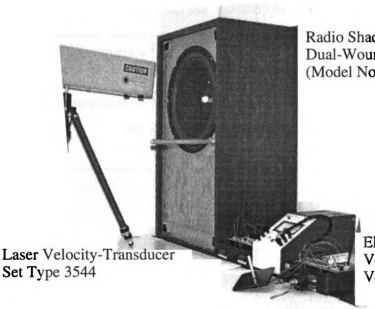

Figure 3.6. Experimental Setup for Speaker Velocity Feedback

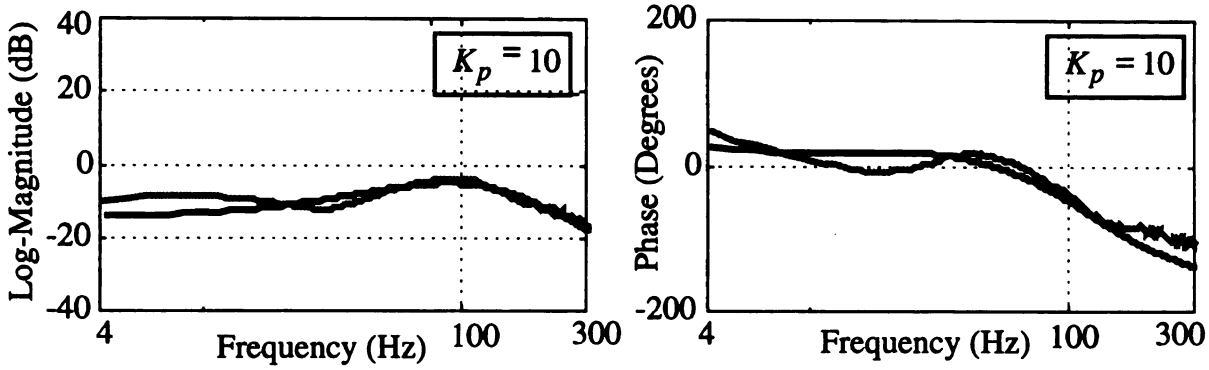

Figure 3.7. Comparison of Measured and Model Closed-Loop Speaker Velocity Response for Proportional Gain of $K_p = 10$ (dB re 1)

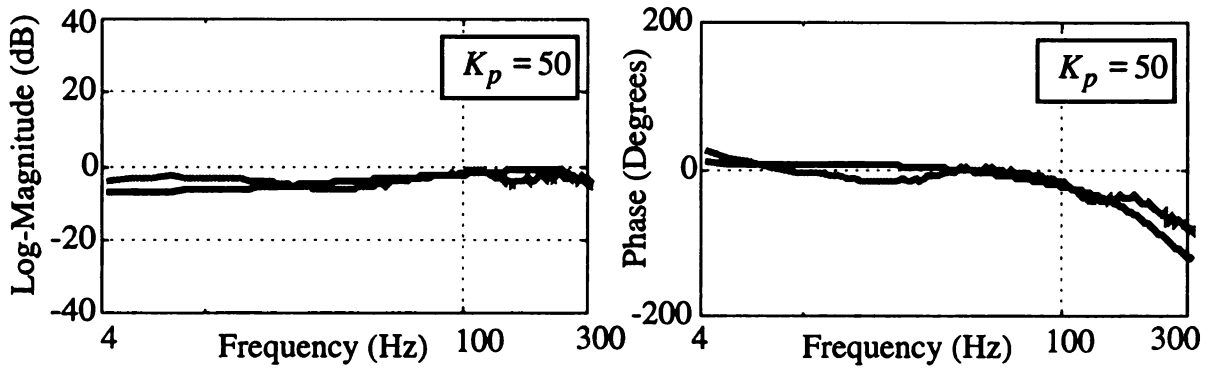

Figure 3.8. Comparison of Measured and Model Closed-Loop Speaker Velocity Response for Proportional Gain of $K_p = 50$ (dB re 1)

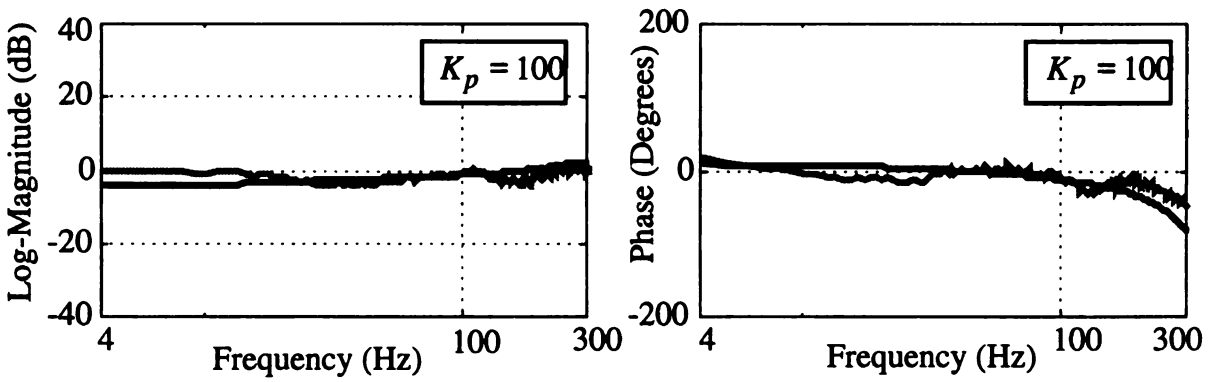

Figure 3.9. Comparison of Measured and Model Closed-Loop Speaker Velocity Response for Proportional Gain of $K_p = 100$ (dB re 1)

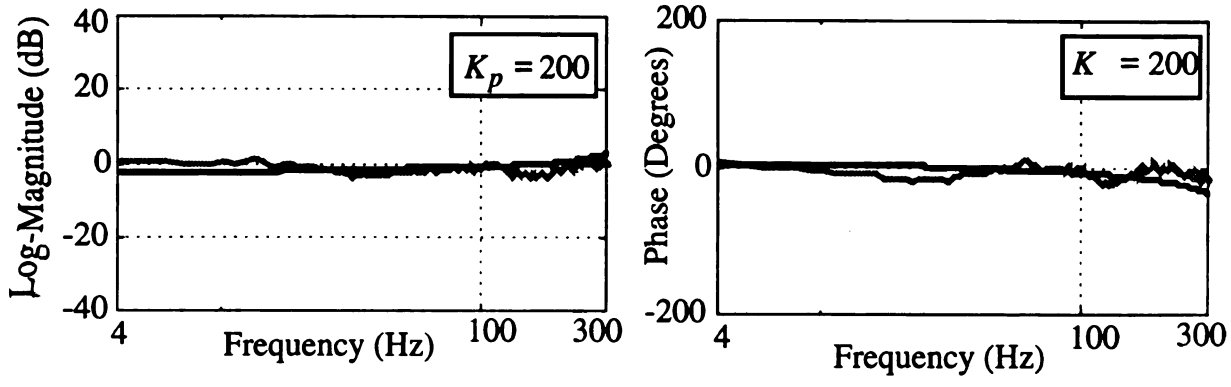

Figure 3.10. Comparison of Measured and Model Closed-Loop Speaker Velocity Response for Proportional Gain of $K_p = 200$ (dB re 1)

The feedback compensation uses simple control technology, is easy to implement and the results are especially significant because no changes in speaker physical parameters are required. Compensation of speaker response allows speaker cone velocity to accurately track desired velocity inputs such as the output of an acoustic controller. It makes limited bandwidth subwoofer speakers effective acoustic control actuators.

3.6. Summary

Velocity feedback compensation for minimizing the magnitude and phase variations in the velocity frequency response of a dual-wound coil subwoofer speaker is presented in this chapter. The feedback compensation uses proportional controller to drive the subwoofer through primary speaker coils. The speaker cone velocity sensing is done by a novel velocity sensor designed using the bond graph model of subwoofer. It uses speaker cone motion induced secondary coil voltage obtained by compensating the mutual inductance effect between dual-wound coils.

Speaker velocity feedback compensation is experimentally shown to reduce speaker velocity magnitude and phase variations. The compensated speaker has variations less than 5 dB in gain and 20 degrees in phase over 4-400 Hz bandwidth compared to 20 dB and 160 degrees variations for the uncompensated speaker. This allows compensated

subwoofer speaker to accurately follow any desired velocity input and makes it an effective acoustic control actuators in AAS.

Chapter 4 Active Acoustic Sink Control Model Development

4.1. Introduction

An analytical model of an AAS controller is developed in this chapter using a compensated speaker model and an acoustic model of enclosed space. The AAS uses velocity compensated speaker to absorb acoustic energy. The speaker compensation is shown to be necessary for the successful performance of AAS. A theoretical analysis is done to show that a negative, real acoustic impedance at the speaker face results in local acoustic power flux into the speaker. The AAS controller is designed to give an acoustically absorptive speaker surface by generating a negative real acoustic impedance at the speaker face. A stability analysis is performed to verify that the controller model results in a stable closed loop AAS system. The resulting controller model provides maximum possible absorption of local acoustic power flux over a wide range of noise frequencies without destabilizing the AAS system.

4.2. Theory of Active Acoustic Sink System

Theoretical analysis shows that a negative, real acoustic impedance at the speaker face results in local acoustic intensity directed into the speaker. An Intensity analysis based on an acoustic energy balance equation is applied here to a control volume containing an electromechanical speaker. It accounts for the rate of change of acoustic energy within a volume, rate of acoustic energy outflow from the volume and power radiated by any sources within the control volume.

Consider a closed, piecewise smooth surface, S, bounding the control volume, V which encloses an electromechanical speaker (Figure 4.1). An area element of surface S is denoted by dS with an outward unit normal vector, $\vec{n}$. The speaker with a source strength of $\frac{q_{spkr}}{V_s}$ is idealized as a monopole flow source located at $\boldsymbol{x_o}$ in the control volume.

$$\frac{q_{spkr}}{V_s} = \frac{A_{spkr} v_{spkr}}{V_s} \tag{4.1}$$

where, A_{spkr} is the effective area of speaker cone and v_{spkr} is the speaker cone velocity. V_s is the volume of a pulsating sphere whose flow rate is equivalent to the volumetric flow rate introduced by the speaker cone motion.

The principles of mass and momentum conservation applied to the control volume result in following vector equations

$$\frac{1}{c^2}\frac{\partial p}{\partial t} = -\rho_o \vec{\nabla} \bullet \vec{v} + \rho_o \frac{q_{spkr}}{V_s} \delta(\boldsymbol{x} - \boldsymbol{x_o}) \tag{4.2}$$

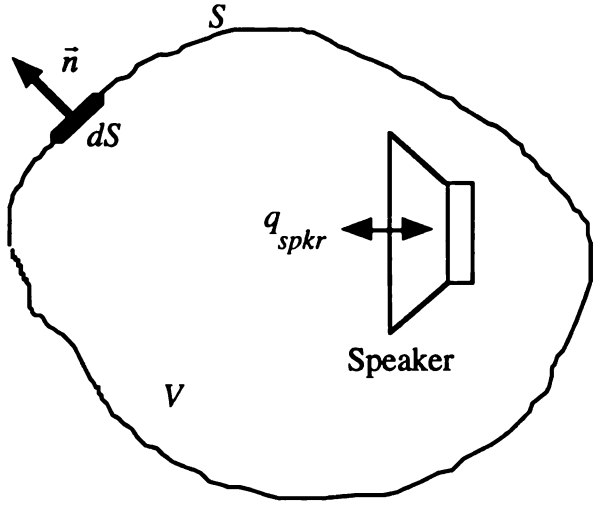

Figure 4.1. Control Volume containing Idealized Point Flow Source

$$\rho_o \frac{\partial \vec{v}}{\partial t} + \vec{\nabla} p = 0 \tag{4.3}$$

where, c is the speed of sound in air, ρ_o is the equilibrium density of air, p is the fluctuation in pressure from its equilibrium value and $\vec{v}$ is the vector of particle velocity fluctuations. $\delta(x - x_o)$ is the three-dimensional delta function and has properties analogous to the one-dimensional Dirac delta function.

The acoustic energy balance equation can be written by adding the equations obtained by multiplying (4.2) with p/ρ_o and taking the dot product of $\vec{v}$ with (4.3).

$$\frac{\partial E}{\partial t} + \vec{\nabla} \bullet \vec{I} = p \frac{q_{spkr}}{V_s} \delta(x - x_o) \tag{4.4}$$

where $E = \frac{1}{2}\rho_o \left(\vec{v} \bullet \vec{v} + \frac{p^2}{c^2} \right)$ is the acoustic energy density and $\vec{I} = p\vec{v}$ is the acoustic intensity. The first term on the left side of (4.4) represents the rate of change of energy in the control volume while the second term represents the rate of outflow of energy from the control volume. The term on the right side of (4.4) represents a source imparting acoustic energy to the control volume through a "monopole" speaker. Equation (4.4) can thus be interpreted as the acoustic energy conservation law applied to the control volume, V and forms the basis for further analysis. Taking the time-average of (4.4), we get

$$\lim_{T \to \infty} \left(\frac{E(T) - E(0)}{T} \right) + \lim_{T \to \infty} \frac{1}{T} \int_0^T (\vec{\nabla} \bullet \vec{I}) dt = \lim_{T \to \infty} \frac{1}{T} \int_0^T \left(p \frac{q_{spkr}}{V_s} \delta(x - x_o) \right) dt \tag{4.5}$$

Noting that the acoustic energy density, $E(T)$, inside a control volume is bounded as $T \to \infty$, (4.5) reduces to

$$\vec{\nabla} \bullet \bar{\vec{I}} = \frac{1}{V_s} \overline{p q_{spkr}} \delta(x - x_o) \tag{4.6}$$

where, $\bar{\vec{I}}$ and $\overline{p q_{spkr}}$ denote the time-averages of $\vec{I}$ and $p q_{spkr}$ respectively.

The acoustic power output, W, from the control volume is given by

$$W = \int_S \bar{I} \bullet \bar{n}\, dS \tag{4.7}$$

Using (4.6) and Gauss's divergence theorem, (4.7) can be written as

$$W = \iiint_V \bar{\nabla} \bullet \bar{I} dV = \frac{1}{V_s} \iiint_V \overline{pq_{spkr}} \delta(x - x_o) dV \tag{4.8}$$

The three-dimensional delta function exhibits the "sifting" property for a continuous function, $f(x)$ in three-dimensional space

$$\iiint_V f(x)\delta(x-y)dV = \begin{cases} f(y), & y \text{ within } V \\ 0, & y \text{ outside } V \end{cases} \tag{4.9}$$

Assuming that the time-averaged quantity, $\overline{pq_{spkr}}$ is continuous within the control volume, the relation (4.8) for acoustic power, W, can be written as

$$W = \frac{1}{V_s} \overline{p(x_o) q_{spkr}} \tag{4.10}$$

If the speaker volumetric flow rate, q_{spkr}, is chosen such that it tracks the acoustic pressure, $p(x_o)$, at the speaker face,

$$q_{spkr}(x_o) = -Kp(x_o) \tag{4.11}$$

a negative real speaker face acoustic impedance will result. With the choice of speaker volumetric flow rate in (4.11), the acoustic power output from the control volume is

$$W = -\frac{K}{V_s} \overline{p^2(x_o)} \tag{4.12}$$

For $K > 0$, it is clear from (4.12) that the acoustic power in the control volume will always be negative. This corresponds to power absorbed by the control volume. Any external noise source located near the control volume will have its local acoustic energy directed into the control volume causing it to behave as an active acoustic sink. The electromechanical speaker can thus be made to act as an active acoustic absorber if the AAS controller is designed to realize the control law (4.11). It has been postulated recently (Madanshetty, et al., 1994) that other choices of speaker volumetric flow rate,

q_{spkr}, will result in acoustic power absorption. The derivation above clearly indicates choice of speaker volumetric flow rate in (4.11) is required for acoustic power absorption by the speaker.

The volumetric flow rate of absorptive speaker must track the acoustic pressure at the speaker face as per the control law (4.11). It is critical that this tracking occurs over the controller bandwidth with minimum magnitude and phase error if AAS is to be successfully used for wide band noise control applications. Since the speaker volumetric flow rate is linearly related to the speaker cone velocity according to (4.1), speaker velocity must track the speaker face pressure for (4.11) to be satisfied. It was shown earlier that the cone velocity of a conventional electromechanical speaker cannot accurately follow the desired signal (Figures 2.5-2.6, and Figure 2.8) due to the speaker free air-resonance. This makes conventional electromechanical speakers inappropriate acoustic absorbers unless a compensation is provided for their varying velocity response. A practical method of speaker compensation using velocity feedback was discussed in Chapter 3. The compensated speaker is used as effective control actuator in the AAS.

4.3. Active Acoustic Sink Controller Design

The AAS controller is designed to yield an acoustically absorptive speaker cone surface resulting in local acoustic intensity being directed into the compensated speaker. The block diagram of the AAS system is shown in Figure 4.2. A microphone with a sensitivity of S_{mic} is placed at the speaker face and measures the total acoustic pressure, p_{face} at the speaker face consisting of the pressure components due to the motion of speaker cone surface, p_{spkr}, the pressure component due to incident acoustic waves from ambient noise, p_i and the pressure component due to reflected acoustic waves from the speaker face, p_r.

$$p_{face} = p_{spkr} + p_i + p_r = p_{spkr} + (1 + \Re(\omega))p_i \tag{4.13}$$

where, $\Re(\omega)$ is the pressure-amplitude reflection coefficient defined as the ratio of

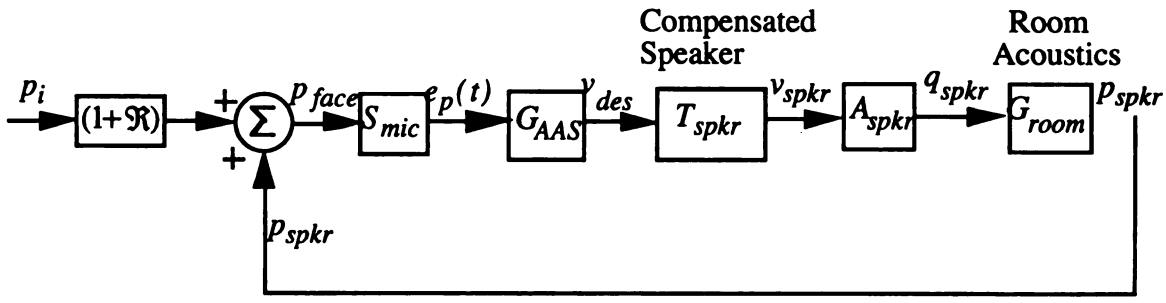

Figure 4.2. Block Diagram of Active Acoustic Sink

Fourier transform of reflected wave pressure, p_r, to the incident wave pressure, p_i (Pierce, 1981). The signal, $e_p(t)$, from the microphone is an input to the AAS controller. The output of the AAS controller transfer function, G_{AAS}, is the desired signal, v_{des}, for the compensated speaker. The volumetric flow rate of the compensated speaker, q_{spkr}, acts through the room acoustics transfer function, G_{room}, to generate the acoustic pressure component, p_{spkr}. This room transfer function generates in a closed loop process. The relation between speaker volumetric flow rate, q_{spkr}, and the speaker face pressure, p_{face} is obtained from the block diagram of the closed loop AAS system.

$$q_{spkr} = (S_{mic} G_{AAS} T_{spkr} A_{spkr}) p_{face} \tag{4.14}$$

The required AAS controller transfer function, G_{AAS}, is obtained by substituting the AAS design objective (4.11) into the system model (4.14) and rearranging terms

$$G_{AAS} = \frac{-K}{S_{mic} A_{spkr} T_{spkr}} \tag{4.15}$$

Since the speaker transfer function, $T_{spkr}(s)$, approaches a real constant, $1/\beta$, at high levels of compensation (Figure 3.10), the AAS controller transfer function simplifies to a pure gain.

$$G_{AAS} = \frac{-K\beta}{S_{mic} A_{spkr}} \tag{4.16}$$

The only non-static terms in (4.16) is the microphone sensitivity, S_{mic}. The radio shack microphone used in the implementation of AAS controller has a nearly constant transfer function in 50-1000 Hz frequency range.

4.4. Stability Analysis of Active Acoustic Sink System

A stability analysis is needed to determine the maximum stable, closed loop controller gain, K, in the presence of room acoustics, G_{room}, and compensated speaker dynamics, T_{spkr}. The closed-loop transfer function, $T_{cl}(s)$, of the AAS system (Figure 4.2) with controller (4.16) is

$$T_{cl}(s) = \frac{P_{spkr}(s)}{P_i(s)} = (1+\Re)\frac{G_{ol}(s)}{1-G_{ol}(s)} = (1+\Re)\frac{-K\beta T_{spkr}(s)G_{room}(s)}{1+K\beta T_{spkr}(s)G_{room}(s)} \tag{4.17}$$

where, $G_{ol}(s)$ is the open-loop transfer function

$$G_{ol}(s) = -K\beta T_{spkr}(s)G_{room}(s) \tag{4.18}$$

The closed-loop system transfer function (4.17) will be unstable if $1-G_{ol}(j\omega)=0$, for any ω. In other words, if the open-loop transfer function is such that

$$K\beta T_{spkr}(s)G_{room}(s) = -1 \quad \text{for } s = \pm j\omega, \forall \omega \geq 0 \tag{4.19}$$

the closed-loop AAS system will be unstable. This can be stated in terms of the usual Nyquist criteria for negative feedback systems by considering $\hat{G}_{ol}(s) = K\beta T_{spkr}(s)G_{room}(s)$ to be a modified open-loop transfer function of the AAS system.

Nyquist Criteria : Let the curve C_2 in complex plane be the mapping of a closed curve, C_1 completely enclosing the right half of the $s-$plane through a stable transfer function, $\hat{G}_{ol}(s)$. If $\hat{G}_{ol}(s)$ is analytic and single-valued within and on C_1 and does not have any poles or zeros on C_1, then the closed loop system (4.17) will be stable provided C_2 does not encircle the critical point $(-1, j0)$.

The stability criteria of closed-loop AAS system as stated in the above theorem can be assessed from the frequency response function, $\hat{G}_{ol}(j\omega)$ since the modified open-loop

transfer function, $\hat{G}_{ol}(s)$, is linear time-invariant, stable and proper. If the frequency response function has a phase which is an integer multiple of -180°, for some frequency, $\omega = \omega_1$, its steady state magnitude will be $\left|\hat{G}_{ol}(j\omega)\right|$, a real constant. The gain, K of the AAS controller in that case can be increased by a factor of $1/\left|\hat{G}_{ol}(j\omega)\right|$ before the curve C_2 encircles the point $(-1, j0)$ and the closed loop AAS system becomes unstable. $\frac{1}{\alpha}$ is the stability gain margin of the AAS system at the phase crossover frequency of ω_1.

The phase crossings of the modified open-loop transfer function, $\hat{G}_{ol}(s)$ at -180°, if any, are obtained by predicting the phase angles of individual transfer function appearing in $\hat{G}_{ol}(s)$. The speaker used as an acoustic absorber when placed in an enclosure is assumed to behave as a circular piston mounted in an infinite baffle. The transfer function, $G_{room}(s)$, between acoustic pressure component, p_{spkr}, and the speaker volumetric flow rate, q_{spkr}, then follows from the following relation for a circular piston (Beranek, 1986)

$$\frac{p_{spkr}}{q_{spkr}}(j\omega) = G_{room}(j\omega) = \frac{\rho_o c}{A_{spkr}}\left[1 - \frac{J_1(2kr_{spkr})}{kr_{spkr}}\right] + \frac{j\rho_o c}{2(kA_{spkr})^2} K_1(2kr_{spkr}) \quad (4.20)$$

where, $k = \frac{\omega}{c}$ is the wave number. J_1 and K_1 are the Bessell functions represented by the series

$$J_1 = \frac{x}{2} - \frac{x^3}{2^2 \cdot 4} + \frac{x^5}{2^2 \cdot 4^2 \cdot 6} - \frac{x^7}{2^2 \cdot 4^2 \cdot 6^2 \cdot 8} \cdots\cdots \quad (4.21)$$

$$K_1(x) = 2\left(\frac{x^3}{3} - \frac{x^5}{3^2 \cdot 5} + \frac{x^7}{3^2 \cdot 5^2 \cdot 7} \cdots\cdots\right) \quad (4.22)$$

where $x = 2kr_{spkr}$. r_{spkr} is the effective radius of the speaker and equal to 66% of the advertised nominal radius of the speaker. At low frequencies where $kr_{spkr} << 2$, the reactive component of (4.20) is dominant and the first two terms of the $J_1(x)$, and $K_1(x)$ series are sufficient to express it (Colloms, 1985). This simplifies the room transfer

function, G_{room}, to

$$G_{room}(s) = \left(\frac{8\rho_o}{3\pi^2 r_{spkr}}\right) s \tag{4.23}$$

The room acoustics thus has a constant 90° phase. The transfer function, G_{room}, was measured with the enclosed, 12 inch, dual-wound coil subwoofer speaker (Radio Shack model 40-1350) and compares reasonably well with the response of theoretical model (4.23). The measured magnitude response has 20 dB/decade slope (Figure 4.3) and measured phase response is close to 90° suggesting a transfer function of the form (4.23) for room acoustics. For an enclosed speaker, the speaker cone motion is affected by the enclosure at the back and the assumption that an enclosure acts as an infinite baffle is not very accurate. This introduces inaccuracies in the theoretical model causing differences between measured and theoretical response of room acoustics. The closed loop transfer function, $T_{spkr}(s)$, of the compensated speaker approaches a real constant at high proportional gains and does not contribute to the phase of modified open-loop transfer function. The sensitivity of the microphone, S_{mic}, and controller transfer function, G_{AAS} (4.16) are both real constants and hence have 0° phase. Therefore, the modified open-loop transfer function theoretically has a constant 90° phase. It does not cross -180° at any frequency giving an infinite gain margin for the closed-loop system. In theory, the active acoustic sink controller model (4.16) will thus yield a stable closed-loop AAS system for any $0 < K < \infty$. It must be noted here that any unmodeled or unstable high frequency dynamics of the compensated speaker and room acoustics will reduce the gain margin and thereby limit the gain of AAS controller.

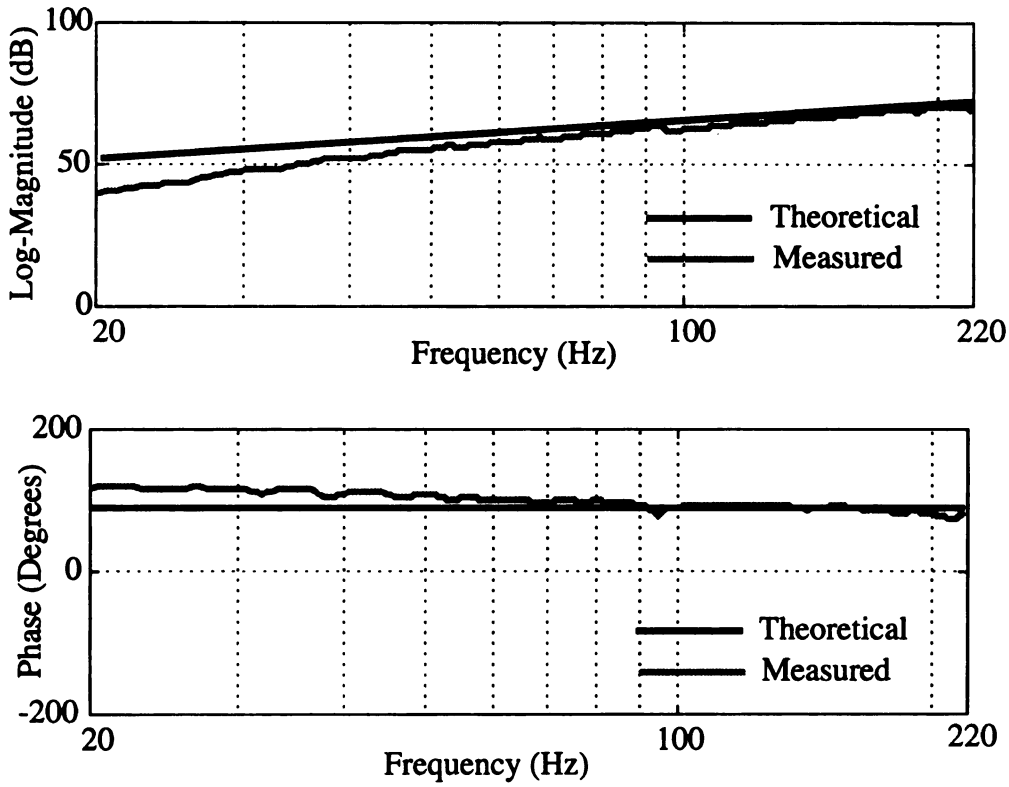

Figure 4.3. Comparison of Theoretical and Measured Magnitude Response of Room Acoustics (dB re 1 Pa-sec/m)

4.5. Summary

An analytical Active Acoustic Sink (AAS) controller model was developed in this chapter to achieve an acoustically absorptive surface at the face of a speaker cone. It provides acoustic power absorption over a wide range of noise frequencies by directing local acoustic power flux into the speaker. A negative real acoustic impedance at the speaker face is shown to be necessary for an acoustically absorptive surface. It was also shown that speaker compensation is necessary for the successful performance of AAS. A stability analysis was done to verify that the resulting AAS controller results in a stable closed-loop system.

Chapter 5 Implementation and Testing of Active Acoustic Sink Controller

5.1. Introduction

The implementation and testing of the AAS system is discussed in this chapter. The AAS controller gain is chosen using the gain margin of the open loop AAS system. The AAS controller is implemented using a velocity compensated speaker to provide maximum possible absorption of local acoustic power flux over 65-200 Hz bandwidth. Experimental tests of the AAS indicate successful performance.

5.2. Implementation of Active Acoustic Sink Controller

The AAS controller is implemented with the controller gain obtained from the gain margin of open loop AAS system. The open-loop configuration shown in Figure 5.1 is obtained by breaking the measured pressure path and inserting a reference voltage, $r(t)$. The frequency response of the modified open-loop transfer function, $\hat{G}_{ol}(s) = \left(\frac{K\beta}{S_{mic}A_{spkr}}\right) T_{spkr}A_{spkr}G_{room}$, from reference signal, $r(t)$, to microphone signal, e_p, is measured for $\left(\frac{K\beta}{S_{mic}A_{spkr}}\right) = 1$. An enclosed, compensated 12-inch diameter, dual-wound coil subwoofer speaker (Radio Shack Realistic model 40-1350) is used to measure the frequency response of transfer function. The effective speaker area, A_{spkr}, of the dual-wound subwoofer is 0.03 m^2 and the value of β used was 6. The speaker face pressure was measured by a microphone (Radio Shack Model 33-1052; sensitivity, $S_{mic} = 4$ mv/Pa) placed at a distance of 18 cm from the speaker face. The measured open-loop frequency response (Figure 5.2) shows an infinite phase margin and a 19 dB

gain margin at the phase-crossover frequency of 813 Hz. The AAS gain, K, can therefore be increased from its open-loop value of 2.1×10^{-5} by a factor of 8.9 (19 dB) before destabilizing the closed loop AAS system. A gain of 10^{-4} meets the recommended 6 dB gain margin and 30-60° phase margin requirement for SISO closed loop system (Ogata, 1986) and was chosen to implement the AAS system.

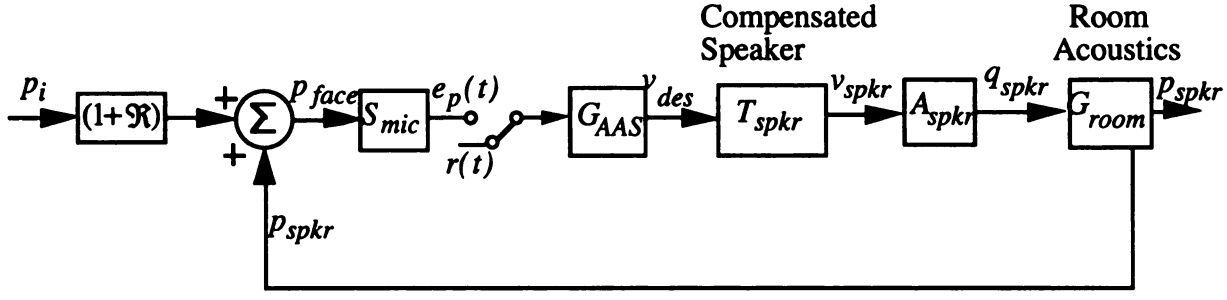

Figure 5.1. Open-Loop Configuration of Active Acoustic Sink System

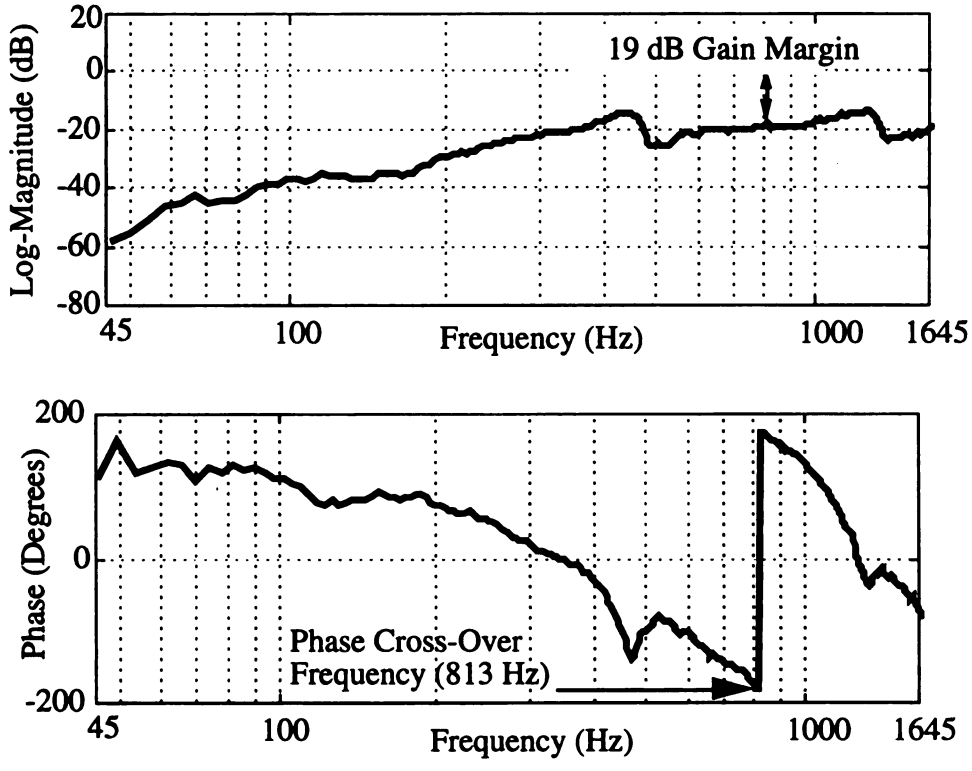

Figure 5.2. Bode Diagram of Open Loop Active Acoustic Sink System (dB re 0.004)

The distance of microphone from the speaker face is critical in the selection of AAS controller gain as it affects the gain margin of the system. As the microphone is moved closer to the speaker face, the open loop gain of the system increases thereby reducing the available gain margin. The microphone should therefore be moved away from the speaker face to increase the AAS absorber gain. The AAS design objective (4.12) requires the speaker volumetric flow rate due to speaker cone velocity track acoustic pressure at the speaker face. The pressure measurement should therefore be ideally made at the speaker face. Higher signal levels in the AAS loop also require that microphone be placed closer to the speaker face. These conflicting requirements have to be met while selecting the microphone distance. In our implementation AAS system, microphone was placed 18 cm away from the speaker face to satisfy these requirements. This distance between the microphone and the speaker surface gives rise to a measured phase angle between pressure and speaker cone velocity that is different from the physically correct one. For the propagating part of the sound field from the speaker face, this phase difference can be estimated from the propagation speed of sound, c, and the distance, Δx, between speaker cone and diaphragm of the microphone. The time required by the sound wave to travel the distance Δx results in an estimated phase shift, $\Delta\phi_x$.

$$\Delta\phi_x = \left(\frac{360}{c}\right) \times f \times \Delta x \quad \text{(in degrees)} \tag{5.1}$$

The phase shift is proportional to frequency, f (Hz) and the distance, Δx. For a distance of $\Delta x = 18$ cm, used in our AAS system implementation, this phase shift is considerable even at small frequencies as seen from Figure 5.3. A phase shift correction is therefore necessary to evaluate AAS system performance at the speaker face.

5.3. Performance Evaluation of Active Acoustic Sink System

The performance of AAS system is evaluated by three independent methods: speaker face impedance, the acoustic energy absorbed at the speaker face, and the P-I index defined as the ratio of sound pressure level at the speaker face to acoustic intensity.

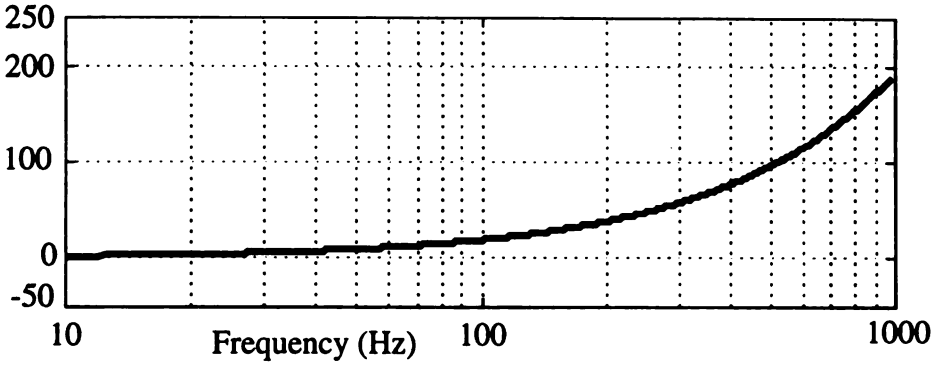

Figure 5.3. Phase Shift, $\Delta\phi_x$, due to Finite Distance between Microphone and Speaker Cone

These three methods will be discussed in detail below.

The speaker face impedance, Z, is the transfer function from speaker volumetric flow rate, q_{spkr}, to speaker face pressure, p_{face}, and provides the first criteria for evaluating the effectiveness of the AAS system. It is in general a complex quantity at any given frequency

$$Z(f) = \frac{P_{face}}{Q_{spkr}} = R(f) + iX(f) \tag{5.2}$$

The real part, $R(f)$, is the acoustic resistance and represents the in-phase, non-conservative, energy transfer at the speaker face. The imaginary part, $X(f)$, is the acoustic reactance and represents the out-of-phase, conservative, energy transfer at the speaker face. For negative acoustic resistance, acoustic energy will be absorbed at the speaker face. The AAS objective (4.12) requires speaker face impedance to be pure real and negative for absorption of incident acoustic power.

$$Z = \frac{-1}{K} \tag{5.3}$$

Using (4.12) and (5.3), more acoustic energy will be absorbed at the speaker face as the

negative real speaker face impedance becomes smaller in magnitude. The speaker face acoustic resistance should therefore be negative and speaker face acoustic reactance ideally be zero for perfect absorption of acoustic power. Any non-zero, negative speaker face resistance, will result in net energy absorption by the AAS independent of speaker face reactance.

Speaker face acoustic impedance was measured (Figure 5.4) for two independent cases to evaluate the effectiveness of the AAS. An enclosed subwoofer used as noise source generated acoustic noise of constant amplitude over the 65-200 Hz bandwidth of the test. The measurement of disconnected speaker impedance with no applied control (uncontrolled system) (Figure 5.5) has a 22 dB gain and 100° phase variation over 65-200 Hz bandwidth. The measurement of AAS impedance with the controlled, compensated speaker (controlled system) (Figure 5.6) shows a 9.6 dB gain and 40° phase variation over the same bandwidth. The acoustic impedance is nearly negative real and has smaller magnitude over this frequency range for the controlled system indicating that it is possible to absorb more acoustic energy with the controlled, compensated speaker. At frequencies below 100 Hz, the real and imaginary parts of the speaker impedance are comparable for both the controlled and uncontrolled systems. Therefore, a little change in the acoustic energy absorbed from uncontrolled to controlled state is expected below 100 Hz. At frequencies above 100 Hz, the imaginary part of the speaker impedance dominates for the uncontrolled system while speaker impedance is nearly negative real for the controlled system and a larger increase in energy absorption is expected.

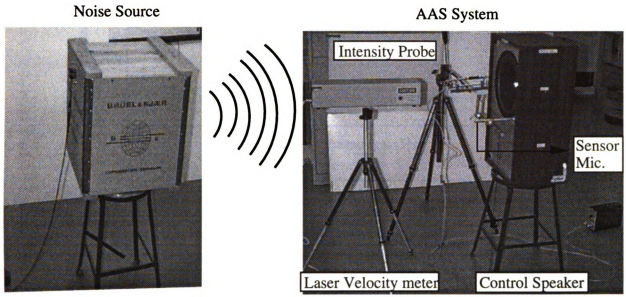

Figure 5.4 Active Acoustic Sink Experimental Setup

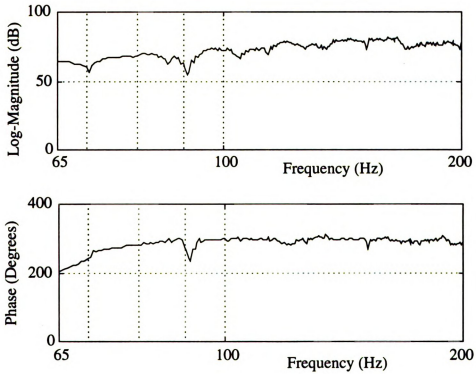

Figure 5.5. Speaker Impedance of Uncontrolled AAS System (dB re Pa-sec/m^3)

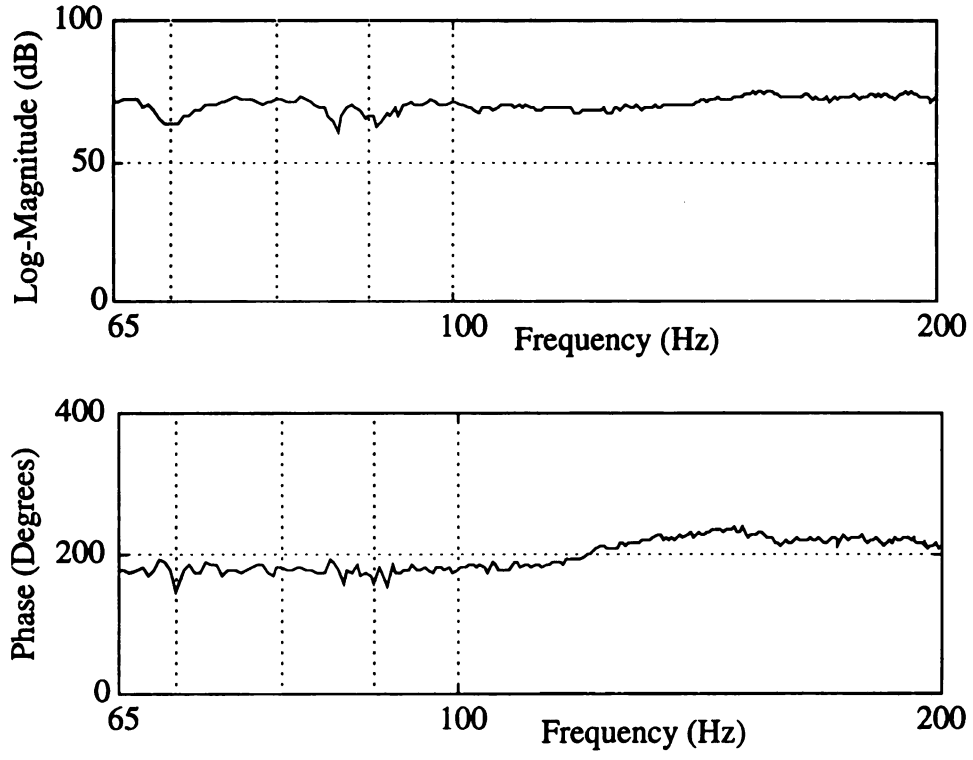

Figure 5.6. Speaker Impedance of Controlled AAS System (dB re Pa-sec/m^3)

The change in acoustic energy absorbed with frequency can be derived from the relationship between variation in acoustic intensity with magnitude and phase of the speaker impedance. The time-averaged acoustic intensity at the speaker face is the time-averaged flow of acoustic energy across a unit surface area of the speaker. It can be written as

$$\mathbf{I} = \frac{1}{2T}\int_{-T}^{T} p_{face}(t)v_{spkr}(t)dt = \frac{1}{2TA_{spkr}}\int_{-T}^{T} p_{face}(t)q_{spkr}(t)dt \qquad (5.4)$$

where, $p_{face}(t)$ is the instantaneous value of acoustic pressure, $q_{spkr}(t)$ is the instantaneous value of speaker volumetric flow rate due to speaker cone velocity, $v_{spkr}(t)$ measured in direction normal to speaker cone surface. For a sinusoidal variation of

magnitude α in the speaker face pressure, $p_{face}(t) = \alpha \sin(\frac{2\pi}{T}t)$, the speaker volumetric flow rate is, $q_{spkr}(t) = \gamma \sin(\frac{2\pi}{T}t + \phi)$. $\gamma = \alpha K$ is the amplitude of the speaker volumetric flow rate. $1/K$ and ϕ are the magnitude and phase of the speaker face impedance at frequency of $1/T$ Hz. The acoustic intensity can then be written as

$$\mathbf{I}(f) = \frac{\alpha^2 K}{2TA_{spkr}} \int_{-T}^{T} \sin(\frac{2\pi}{T}t) \sin(\frac{2\pi}{T}t + \phi) dt \tag{5.5}$$

$$\therefore \mathbf{I}(f) = \frac{\alpha^2}{2A_{spkr}} \times K \cos\phi = \frac{\gamma^2}{2A_{spkr}} \times \frac{1}{K} \times \cos\phi \tag{5.6}$$

For a constant amplitude, γ, of speaker volumetric flow rate, the change in acoustic intensity with frequency is proportional to the change in speaker impedance magnitude and phase. The variation in absorbed acoustic energy with frequency in controlled and uncontrolled AAS system can thus be predicted from the speaker impedance curves (Figures 5.5-5.6) and the phase correction curve (Figure 5.3). For example, the uncontrolled impedance magnitude changes from 4731.5 (73.5 dB) to 8912.5 (79 dB) from 111 Hz to 145 Hz. The phase angle is nearly constant at 268° after correction for propagation phase shift at these frequencies. An increase of 2.75 dB in absorbed acoustic energy is therefore expected from 111 Hz to 145 Hz. Over the same frequency range, the controlled impedance magnitude changes from 2387.32 (67.56 dB) to 4774.65 (73.58 dB) while the adjusted phase changes from 163° to 191°. An increase of 3.1 dB in absorbed acoustic intensity is expected for controlled system from 111 Hz to 145 Hz.

Acoustic energy absorbed by the AAS system was measured to demonstrate its performance (Figure 5.4). A Brüel & Kjaer sound intensity probe (Type 3519) was used to measure acoustic intensity at the front of the speaker for both the uncontrolled and controlled systems. In each test, the acoustic power absorbed by the AAS was indicated by the time-averaged acoustic intensity vector, **I**, into the speaker. These two measurements allowed an independent evaluation of the control performance because the

acoustic energy absorbed in the uncontrolled state was only due to the mechanical dissipation of the speaker.

Acoustic intensity measurements below 70 Hz were demonstrated unreliable due to small pressure signal levels and are not included here. At these frequencies, the measured open-loop response magnitude is less than -45 dB (Figure 5.2). This makes the effect of noise dominant below 70 Hz and accordingly measurements below 70 Hz were found unreliable due to poor signal-to-noise ratio and verified by poor measured coherence below 70 Hz (Figure 5.7).

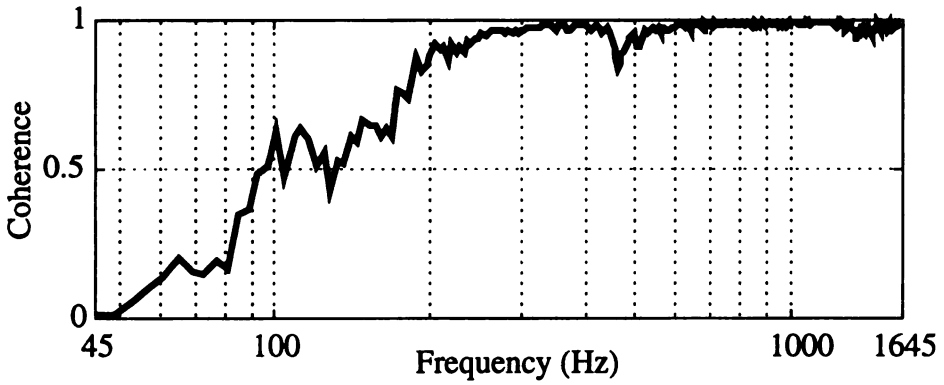

Figure 5.7. Measured Coherence in the Open Loop Frequency Response of AAS

The acoustic energy absorbed in the controlled state by the AAS (Figure 11 and Table 5.1) shows a substantial increase over the uncontrolled state. The percent increase ranges from 12.95% over 70.5-80 Hz to 143.78% over 170.5-180 Hz. This was expected since the impedance of controlled speaker is more nearly negative real over a wider frequency range (Fig. 9). The measured acoustic energy absorbed from 111 Hz to 145 Hz increases by 2.74 dB in uncontrolled state and agrees well with the 2.75 dB increase predicted from the uncontrolled speaker impedance measurements. Over the same frequency range, the increase in acoustic energy absorbed in controlled state is 2.4 dB and

is close to an increase of 3.1 dB predicted from the controlled speaker impedance.

The measurement of P-I index is the final method to check the effectiveness of the AAS system. It is defined as

$$\delta_{PI} = 10\log\left[\frac{\overline{p^2}}{\mathbf{I}}\right] - 10\log[\rho c] \tag{5.7}$$

It is related to the ratio of sound pressure level to intensity and allows the evaluation of the AAS system with reference to the speaker face pressure. The increase in absorbed acoustic energy from uncontrolled to controlled state was calculated from the P-I index (Table 5.2). It compares well with the increase in absorbed acoustic energy measured by the Brüel & Kjaer sound intensity probe.

The acoustic intensity measurements demonstrate the effectiveness of AAS and verify the requirement that speaker impedance must be negative real for acoustic energy to be absorbed into the speaker. The acoustical effect of this would be a high absorption of acoustic energy into the speaker. The AAS system developed in this work can provide an alternate solution to the problem of noise reduction in an acoustic space. Several acoustic sinks can be placed in an acoustic space to absorb acoustic energy.

Table 5.1 Acoustic Energy absorbed by the Active Acoustic Sink

Frequency Band (Hz)	Acoustic Intensity for Uncontrolled system (pW/m^2)	Acoustic Intensity for Controlled system (pW/m^2)	Net Increase in Acoustic Intensity (pW/m^2)	Percent Increase
70.5-80	3981.07	4496.763	515.69	12.95 %
80.5-90	3311.31	3993.93	682.61	20.61 %
90.5-100	2460.37	2726.47	266.09	10.82 %
100.5-110	2902.69	4971.64	2068.96	71.28 %
110.5-120	5318.63	12589.25	7270.62	136.70 %
120.5-130	7216.06	19760.59	12544.54	173.84 %
130.5-140	8757.90	25038.02	16280.12	185.39 %
140.5-150	10000.00	21877.62	11877.62	118.78 %
150.5-160	6444.66	17422.08	10977.42	170.33 %
160.5-170	4075.68	11220.185	7144.51	175.30 %
170.5-180	3512.37	8562.4885	5050.12	143.78 %

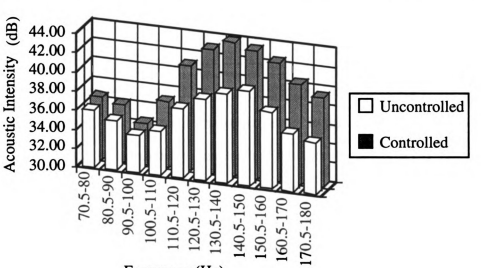

Figure 5.8. Acoustic Intensity Absorbed by AAS in uncontrolled and controlled states

Table 5.2 Increase in Absorbed Acoustic Intensity from Uncontrolled to Controlled States

Frequency Band (Hz)	From P-I Index (dB)	From Intensity Probe (dB)
70.5-80	0.53	0.72
80.5-90	0.81	1.01
90.5-100	0.45	0.43
100.5-110	2.34	2.04
110.5-120	3.74	4.06
120.5-130	4.37	3.61
130.5-140	4.56	5.15
140.5-150	3.4	4.15
150.5-160	4.32	4.86
160.5-170	4.4	3.23
170.5-180	3.87	4.24

5.4. Summary

The AAS system was constructed and its performance evaluated using a velocity compensated, enclosed, dual-wound subwoofer speaker in this chapter. The effectiveness of AAS system was evaluated by measuring speaker impedance in uncontrolled (disconnected speaker with no applied control) and controlled states (controlled, compensated speaker). The measured impedance phase was corrected to account for phase shift introduced due to microphone-laser velocimeter configuration used to measure impedance. The controlled speaker impedance magnitude varied by 9.6 dB and its phase changed from 165° to 200° after correcting for propagation phase shift over 65-200 Hz

bandwidth. Over the same bandwidth, the magnitude of uncontrolled speaker impedance varied by 22 dB gain and its adjusted phase varied from 188° to 267°. The controlled speaker impedance is thus nearly negative real indicating it is possible to absorb more acoustic energy with controlled, compensated speaker. The effectiveness of AAS is demonstrated by measuring the increase in acoustic energy absorbed by the uncontrolled and controlled compensated speaker. The results show an increase from 12.95 % over 70.5-80 Hz to 175.3% over 160.5-170 Hz indicating that it is possible to use a compensated speaker for sound power absorption from an acoustic volume.

Chapter 6 Conclusions

6.1. Dissertation Summary

A prototype Active Acoustic Sink (AAS) was designed and constructed to determine if an electronically driven speaker can be built to absorb acoustic energy. To guarantee the flow of acoustic energy into the speaker, the speaker cone velocity must accurately track acoustic pressure in front of the speaker. The varying velocity frequency response of speakers makes them unsuitable as energy absorbers unless they are compensated. Appropriate compensator design requires an accurate speaker dynamic model.

A simple laboratory based methodology for developing a suitable speaker dynamic model has been presented and experimentally verified in laboratory tests on a dual-coil subwoofer speaker. The speaker cone velocity frequency response is shown to have large magnitude and phase variations below 200 Hz. This makes the subwoofer speaker unsuitable actuator for AAS without compensation. This is the first time that a dynamic model of dual-wound coil subwoofer has been developed to include the effect of mutual inductance between dual coils.

Speaker velocity feedback compensation for minimizing the magnitude and phase variations in velocity response has been designed and experimentally verified in laboratory tests on a dual-coil subwoofer speaker. It uses a proportional controller to drive the subwoofer through primary speaker coils. The speaker cone velocity sensing is done by a novel velocity sensor designed using a bond graph model of the subwoofer. It uses speaker cone motion induced secondary coil voltage obtained by compensating the mutual

inductance effect between dual-wound coils. The compensated speaker has variations less than 5 dB in gain and 20 degrees in phase over 4-400 Hz bandwidth compared to 20 dB and 160 degrees variations for the uncompensated speaker. This is the first successful implementation of speaker velocity feedback compensation to date which does not require any external sensor for measuring speaker cone velocity. Compensation of speaker response now allows the speaker volumetric flow rate to accurately follow the speaker face pressure.

An analytical AAS controller model was developed using the compensated speaker model. The controller design objective was to yield an acoustically absorptive speaker cone surface by generating negative real acoustic impedance at the cone surface of compensated speaker. The resulting controller is a pure gain and a closed loop stability analysis was done to determine its maximum stabilizing value. A stability analysis of point feedback acoustic absorption system has been done for the first time in this work.

The AAS system was constructed and its performance evaluated using a velocity compensated, enclosed, dual-wound subwoofer speaker. The effectiveness of AAS system was evaluated by measuring speaker impedance in uncontrolled (disconnected speaker with no applied control) and controlled states (controlled, compensated speaker). The measured impedance phase was corrected to account for phase shift introduced due to microphone-laser velocimeter configuration used to measure impedance. The controlled speaker impedance magnitude varied by 9.6 dB and its adjusted phase changed from 165^{o} to 200^{o} over 65-200 Hz bandwidth. Over the same bandwidth, the magnitude of uncontrolled speaker impedance varied by 22 dB gain and its adjusted phase varied from 188^{o} to 267^{o}. The controlled speaker impedance is thus nearly negative real indicating it is possible to absorb more acoustic energy with a controlled, compensated speaker. The effectiveness of AAS is demonstrated by measuring the increase in acoustic energy absorbed by the uncontrolled and controlled compensated speaker. The results show an increase from 12.95 % over 70.5-80 Hz to 175.3% over 160.5-170 Hz indicating that it is

possible to use a compensated speaker for sound power absorption from an acoustic volume. This is an improvement over the results obtained by Hall (1994) with his AAS which was limited due to ineffective speaker cone velocity sensor. The AAS uses simple control technology, is easy to implement, and does not require any changes in the physical parameters of the system components.

6.2. Directions for Future Work

There are several areas for future work or improvement in the method stated in this work. The most obvious next step would be to test the effectiveness of AAS in a three-dimensional enclosure such as a vehicle interior. Effective three-dimensional noise control can also be beneficial in the aircraft industry and factories.

The performance of AAS can be improved further by investigating different AAS control algorithms. The weak signal levels at low frequencies in the AAS loop did not allow for good coherent measurements below 65 Hz. The AAS controller can be modified to increase the open loop low frequency gain of the AAS system without changing the high frequency behavior. This might improve the low frequency performance of the system. Another area of improvement is in the measurement of local acoustic intensity at the speaker face of AAS system at low frequencies. The two microphone probe used to measure the intensity cannot be used effectively below 40 Hz. The amount of acoustic power absorption can also be increased by placing more AAS systems.

BIBLIOGRAPHY

Bao, C., Sas, P., Van Brussel, H., 1991, "Active Control of Engine-Induced Noise inside Cars", *Proc. InterNoise 91,* pp. 525-528.

Beranek, L.L., 1986, *Acoustics*, American Institute of Physics, Inc., New York, NY.

Colloms, M., 1985, *High Performance Loudspeakers*, John Wiley & Sons, NY.

Conover, W.B., 1956, "Fighting Noise with Noise", Noise Control, **2**, pp. 78-82.

Costin, M.H., Elzinga, D.R., 1989, "Active Reduction of Low-Frequency Tire Impact Noise Using Digital Feedback Control", *IEEE Control Systems Magazine*, pp. 3-6.

Crocker, M.J., Kessler, F.M., 1982, *Noise and Vibration Control*, Vol. II, CRC Press.

Elliot, S.J., Stothers, I.M., Nelson, P.A., McDonald, A.M., Quinn, D., Saunders, T., 1988, "The Active Control of Engine Noise Inside Cars", *Proc. InterNoise 88,* pp. 971-974.

Elliot, S.J., Nelson, P.A., Sutton, T., McDonald, A.M., Quinn, D., Stothers, I.M., Moore, I., 1990, "The Active Control of Low Frequency Engine and Road Noise Inside Automotive Interiors", *ASME WAM Symposium on Active Noise and Vibration*, pp. 125-129.

Eriksson, L.J., Allie, M.C., Bremigan, C.D., Gilbert, J.A., 1988, "The Use of Active Noise Control for Industrial Fan Noise", ASME Winter Annual Meeting, Chicago, Paper number 88-WA/NCA-4.

Guicking, D., 1990, "On the Invention of Active Noise Control by Paul Leug",

Journal of Acoustical Society of America, **87**, pp. 2251-2254.

Hall, G., "The Development of an Acoustic Energy Absorber for Noise Control Applications", M.S. Thesis, Michigan State University, 1994

Harwood, H.D., 1974, "Motional Feedback in Loudspeakers", *Wireless World*, Vol. 80, pp. 51-52.

Holdaway, H.W., 1963, "Design of Velocity Feedback Transducer Systems for Stable Low-Frequency Behavior", *IEEE Transactions*, AU-11, pp. 155-173.

Holle, W., 1952, "Gegenkopplung an Lautsprechern", *FunkTechnik*, 7, pp. 490-492.

Hull, A.J., Radcliffe, C.J., Miklavčič, M., MacCluer, C.R., 1990, "State Space Representation of the Nonself-Adjoint Acoustic Duct System", *Journal of Sound and Vibration*, Vol. 112, pp. 483-488.

IEEE Standards committee of Acoustics, Speech, and Signal Processing, 1975, "IEEE recommended Practice for Loudpseaker Measurements", IEEE std 219-1975

Joachim, C.A., Nefske D.J., Wolf Jr., J. A., 1981, "Application of a Structural-Acoustic Diagnostic Technique to Reduce Boom Noise in a Passenger Vehicle", *Society of Automotive Engineers, International Congress and Exposition*, Detroit MI, pp. 1-11.

Klaassen, J.A., de Koning, S.H., 1968, "Motional Feedback with Loudspeakers", *Philips Technical Review*, Vol. 29, No. 5, pp. 148-157.

Ling, M.K., 1993, "Vehicle Interior Noise Control Using Three-Layer Composites With Polyurethane Cores", *Journal of Sound and Vibration*, Vol. 160(1),, pp. 103-109.

Madanshetty, S.I., Chu, B.T., 1994, "Active Sound Extraction for Noise Control", ASME Winter Annual Meeting, Chicago.

Manjal, M.L., Eriksson, L.J., 1988, "An Analytical, One-Dimensional, Standing-Wave Model, of a Linear Active Noise Control System in a Duct", *Journal of the Acoustical Society of America*, Vol. 84(3), pp. 1986-1093.

Ogata, K., 1986, *Modern Control Engineering*, Prentice Hall of India.

Olson, H.F., May, E.G., 1953, "Electronic Sound Absorber", *Journal of Acoustical Society of America*, **25**, pp. 1130-1136.

Pierce, A.D., 1981, *Acoustics : An Introduction to Its Physical Principles and Applications,* McGraw-Hill Book Company.

Radcliffe, C.J., Gogate, S.D., 1996, "Velocity Feedback Compensation of Electromechanical Speakers for Acoustic Applications", Submitted for *1996 International Federation of Automatic Control*, San Francisco.

Radcliffe, C.J., Gogate, S.D., 1995, "An Analytical Active Acoustic Sink Controller Model for Wide Band Noise Control Applications", Accepted for presentation at the *ASME Winter Annual Meeting*, San Francisco.

Radcliffe, C.J., Gogate, S.D., Hall, G., 1994, "Development of an Active Acoustic Sink (AAS) for Noise Control Applications", *ASME Winter Annual Meeting Symposium on Active Control of Noise and Vibration,* Vol. 75, pp. 43-50

Radcliffe, C.J., Gogate, S.D., 1992, "Identification and Modeling of Speaker Dynamics for Noise Control Applications", *ASME Winter Annual Meeting Symposium on Active Control of Noise and Vibration*, Vol. 38, pp. 295-300.

Rosenberg, R.C., Karnopp, D.C., *Introduction to Physical System Dynamics*, McGraw-Hill Publishing Company, 1983

Shuku, T., Yoshida, A., Nagai, M., Watari, A., 1972, "Reduction of Interior Car Noise By Control of Cavity Resonance", *14th International Automobile Technical Congress*, London, pp. 56-62.

Sutton, T.J., Elliot, S.J., Nelson, P.A., 1990, "The Active Control of Road Noise inside Vehicles", *Proc. InterNoise 90*, pp. 1247-1250.

Swinbanks, M.A., 1973, "The Active Control of Sound Propagation in Long Ducts", *Journal of Sound and Vibration*, Vol. 27(3), pp. 411-436.

Tanner, R.L., 1951, "Improving Loudspeaker Response with Motional Feedback", *Electronics*, Vol. 24, No. 3.

Warner, J.V., Waters, D.E., Bernhard, R.J., 1988, "Digital Filter Implementation of Local Active Noise Control in a Three Dimensional Enclosure", *ASME Winter Annual Meeting*, Chicago, Paper number 88-WA/NCA-6.

Werner, R.E., 1958, "Loudspeakers and Negative Impedances", *IRE Transactions*, AU-6, pp. 83-89.